이학박사 학위논문

Electrical Properties of Hydrogen-Exposed Single-Walled Carbon Nanotubes

수소에 노출된 단겹 탄소나노튜브의 전기적 특성

2020 년 8 월

서울대학교 대학원

물리천문학부 물리학 전공

강 호 진

Electrical Properties of Hydrogen-Exposed Single-Walled Carbon Nanotubes

Hojin Kang

Supervised by

Professor Yung Woo Park

A Dissertation
Submitted to the Faculty of
Seoul National University
in Partial Fulfillment of
the Requirements for the Degree of
Doctor of Philosophy
August 2020

Department of Physics and Astronomy
Graduate School
Seoul National University

Abstract

Carbon nanotube (CNT) is one of the most promising materials for the next generation electronics. However, there still have been many challenges for the realization of CNT-based electronics. Especially, the hole-favored electronic property of CNT in ambient condition has been the huge obstacle. To form an integrated circuit for logic computation, both *n*-type and *p*-type transistors are necessary. Hence, reliably working *n*-type CNT transistors have been desired.

We report changes in the electrical property of single-walled carbon nanotube (SWNT) caused by exposure to high-pressure hydrogen gas. First, we report the electron doping effect of SWNT. *In-situ* 3-terminal electrical measurements with hexagonal boron nitride (hBN) substrate were used to observe the intrinsic electronic properties of hydrogen-exposed SWNT. Comparing to the planar graphene sheet device, we observed the curved structure of SWNT is advantages on the reaction with hydrogen molecules. X-ray photoelectron spectroscopy (XPS) and Raman spectroscopy verified the formation of C-H bond on SWNT surface after the hydrogen exposure process. The covalent bond yielded short-range scattering in the graphene device and band gap widening in the SWNT devices.

Second, the metal work function-dependent doping effect on SWNT field effect transistor (FET) is investigated. To obtain the SWNT FET with higher Schottky barrier (SB) for the hole injection, we adapted the different contact metals that have lower work functions such as Cr and Ti replacing the Au/Ti electrodes. Comparing to the Au/Ti-contacted SWNT FET case, we observed noticeable hole carrier

reduction after the hydrogen exposure in Cr- and Ti-contacted devices. It suggest the doping induced SB thickness change relies on the SB height. In other words, the changes in thickness (*via* electron doping) of higher SB (*via* low work function metal contact) causes more significant effect on the I_{ds}-V_{gs} curve. Consequently, we achieved the SWNT FET that nearly perfectly working as an *n*-type semiconductor by hydrogen exposure to SWNT FET with Ti contacts.

Since the electron doping effect was also reproduced in SWNT network devices, we expect the useful electrical properties and the stable nature of C-H bond observed in the hydrogen-exposed SWNT can leads a step forward to the application of SWNT for the next generation electronics.

Keywords : Carbon nanotube, hydrogenation, electron doping, *n*-type transistor, electrical measurements, electrical contact, Schottky barrier

Student Number : 2012-23086

Contents

List of figures

List of tables

Chapter 1

Introduction

1.1 Introduction of carbon nanotubes

After great success of Si-based electronics, we are facing the end of Moore's law era saying that the number of transistors in integrated circuit doubles every two years [1]. Because of the physical limits such as significant power consumption caused by leakage current and the short channel effect, the transistors cannot be reduced limitlessly. Approaching the quantum mechanical regime, new concept of transistors and materials is desired to replace the Si-based electronics. Carbon nanotube (CNT) is one of the most promising materials for the next generation electronics. After the discovery of the single-walled carbon nanotubes (SWNT) in 1991 by Iijima [2], the one-dimensional material quickly attracted a great research attention. Especially, the high electrical performance such as high mobility [3], current density [4] and on-off ratio [5] made the SWNT fascinating as a replacement of Si in today's electronics. However, there still have been many challenges for the realization of CNT-based electronics such as lack of reliable fabrication technique for scalable high-performance device, high electrical contact

barriers, and difficulty of changing the majority charge carrier. Especially, the hole-favored electronic property of SWNT in ambient condition has been the huge obstacle. To form an integrated circuit for logic computation, both *n*-type and *p*-type transistors are necessary. So, reliably working *n*-type SWNT transistors have been desired.

1.2 Electronic structure of single-walled carbon nanotubes

To understand the electronic properties of single-walled carbon nanotubes (SWNT), we would better start with understanding a sheet of carbon layer, graphene. Graphene is one atom thick carbon sheet with hexagonal lattice. Because carbon is the group IV element in the periodic table, the number of peripheral electron is supposed to be four. There are total four orbitals to be occupied, $2s$, $2p_x$, $2p_y$, and $2p_z$, where $2s$ is the lowest energy state and the others are degenerated above that. However, to form a hexagonal lattice, three orbitals with equal energy (degeneracy) are needed at the ground state. Consequently, $2s$, $2p_x$, and $2p_y$ orbitals hybridize resulting in the three $2sp$ orbitals with degeneracy. Hence the three $2sp$ orbitals forms a covalent bond (σ-bond) with the three nearest carbon atoms building the two-dimensional hexagonal lattice, and the $2p_z$ orbital is occupied by one electron (π electron). Due to the orbital is occupied by only one electron, the half-filled orbital provides relatively free space for the electrons to move quickly. Exceeding 10^6 $cm^2/(V \cdot s)$ electrical mobility of graphene has been reported [6]. The electronic energy band structure of graphene is described in Fig. 1.1.

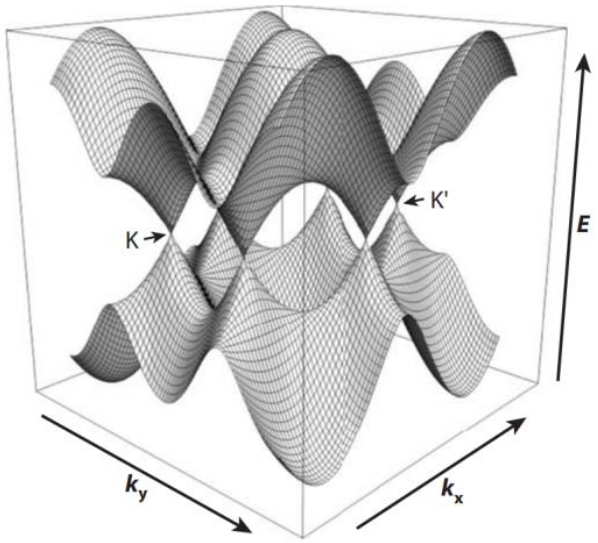

Figure 1.1 Electronic energy band structure of graphene. Adapted from Ref. [7].

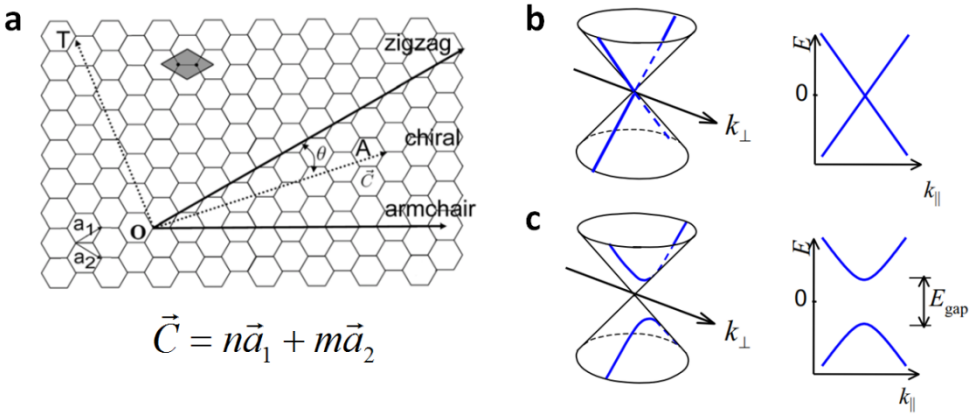

Figure 1.2 Energy band structures of SWNTs. (a) Chirality of SWNT. Image adapted from Ref. [8]. Energy band structures of (b) metallic (c) and

semiconducting SWNTs. (b, c) are adapted from Ref. [9]

As described in Fig. 1.1, the energy band structure of graphene has six-fold symmetry. Therefore, at the Fermi level, there are six points (K-points) where the conduction and valance band meet. Looking into one of the K-points, both conduction and valance bands have cone shape (so called "Dirac cone") meeting at the K-point (so called "Dirac point") as described in left of Figs. 1.2b,c. Because both bands have highly symmetric structure with linear dispersion, the effective mass of electron (which is determined by curvature of energy band) becomes zero. A charge carrier in this regime without effective mass (so called "Dirac Fermion") gives the exotic properties to graphene sheet.

SWNT can be regarded as a rolled graphene strap. Figure 1.2a shows a graphene sheet with the unit vector a_1 and a_2. The chirality of SWNT can be quantified by the chirality vector, $\vec{C} = n\vec{a}_1 + m\vec{a}_2$. Once the graphene strap is rolled up with the chirality vector $\vec{C}$, the electron wave function is confined to $\vec{k}_\perp \cdot \vec{C} = 2\pi i$ (i is an integer) according to the boundary conditions. Figure 1.2b graphically explains the restriction of momentum in the energy band structure. Because the momentum of electron in the SWNT is limited to the certain value of $\left|\vec{k}_\perp\right|$ (left of Fig. 1.2b), cross-section plane perpendicular to $\vec{k}_\perp$ becomes the energy band of SWNT as described right side of Fig. 1.2b. In case the chirality vector fulfills the condition n

- $m = 3i$, the cross-section plane crosses $\left|\vec{k}_{\perp}\right| = 0$. The charge carrier in this semi-metallic energy band structure does not have forbidden energy band, *i.e*. band gap (right side of Fig. 1.2b). Hence the SWNT shows metallic behavior. While, in case of $n - m \neq 3i$, SWNT shows semiconducting behavior with opening the band gap as described in Fig. 1.2c.

1.3 Electrical contact to SWNT and Schottky barrier

Due to the special geometry of carbon nanotubes, quasi 1-dimensional channel, 4-probe electrical measurement technique does not have any advantages. As the metal contacts separate CNT into segments, the independent voltage measurements provided by 4-brobe technique are difficult [10]. Consequently, 2-probe method sharing voltage source and current measurement in the same electrodes are usually performed for the characterization of electronic properties of CNT. Therefore, not only the channel but also contacts play important role in deciding the total electrical property of electronic CNT devices. It brings to a conclusion that study on the interface of SWNT and metal contact is inevitable for the comprehensive understanding on the system.

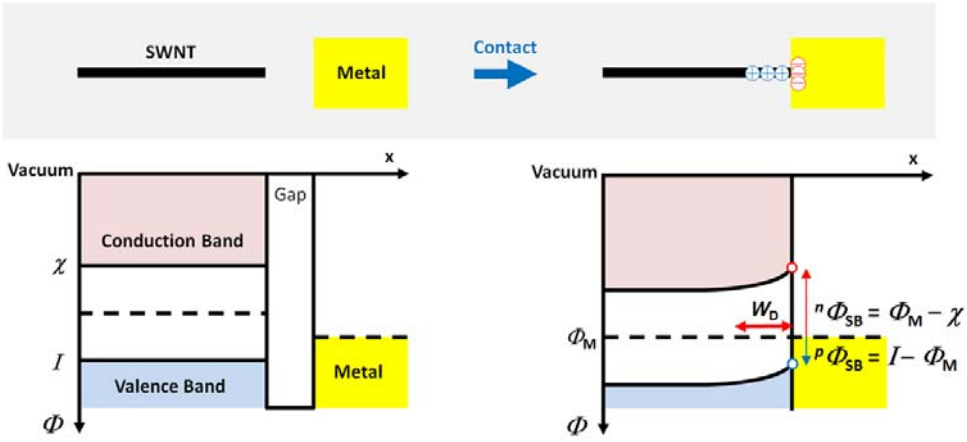

Figure 1.3 Schematic energy diagram of SWNT and high work function metal electrodes with contact.

In the ideal case without surface states, the work function of metal and semiconductor are the two most important factors in formation of Schottky barrier. Left side of Fig. 1.3 shows the schematic energy diagram before the formation of metal-semiconductor junction. The metal with high work function (Φ_M) is aligning with the SWNT having the Fermi-level in the middle of the energy gap [11]. Before they are in contact, there is no interaction. Once they are close enough that the electrons of both sides can interact with each other, it tends to be equilibrium sharing same Fermi-level throughout the system [11]. In other words, the electron of higher Fermi-level material (semiconductor in this case) will flow to the lower Fermi-level material (metal contact). Because metal is regarded as an electron reservoir, the process ends up with the aligning Fermi-level of metal. In the same time, the contact potential of $(\Phi_M - \Phi_{NT})/q$ is built at the interface where the Φ_{NT} is work function of the SWNT and q is the unit charge [12]. Due to the contact

potential, negative charge (in the case of Fig. 1.3) are formed at the metal surface. The negative charges induce positive charges at SWNT making *p-n* junction at the interface. Because the contact potential is determined by the potential of semiconductor with regard to the metal contact, the height of Schottky barrier is defined as ${}^{n}\Phi_{SB} = \Phi_{M} - \chi$ for electron injection, and ${}^{p}\Phi_{SB} = I - \Phi_{M}$ for hole injection [11]. χ is electron affinity of SWNT that is the energy needed to remove an electron from the conduction band minimum. I is ionization energy that represents the energy difference of valence band maximum and vacuum level. However, in case of real devices, there are interface states such as defects on the semiconductor surface, charge traps, and lattice miss match with metal contacts. These interface states make the influence of metal work function on height of SB less effective [12]. Figure 1.4 is the experimental barrier heights for different metals with Si contacts. Without interface states, the SB heights depending on metal work function are supposed to have the slope 1 that represents perfect dependence on metal work function. However, the experimental results show that the slope of SB height dependence on metal work function (c) lies at the somewhere between 0 and 1 where $c = 0$ represents the perfect independence of SB height on metal work function [12].

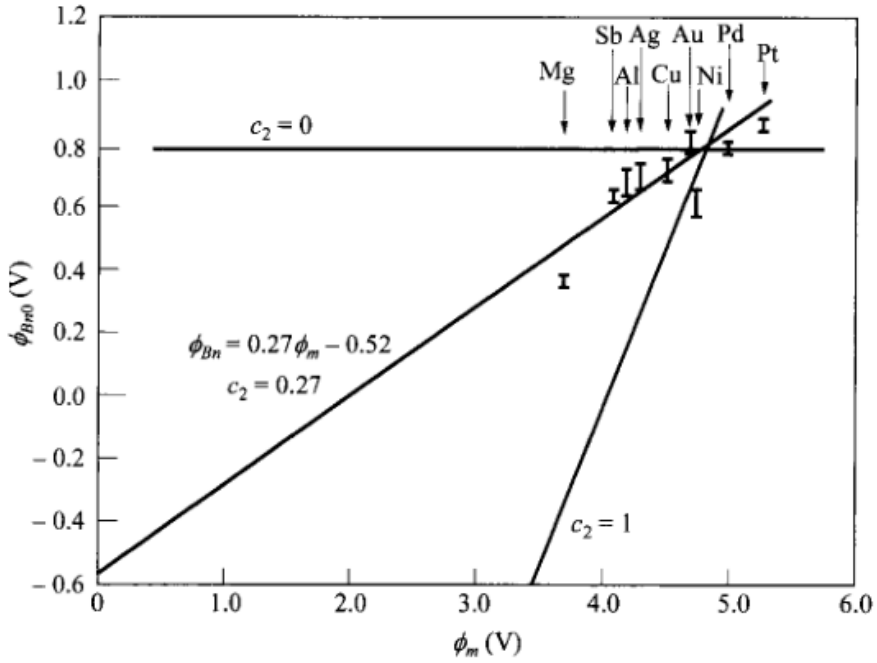

Figure 1.4 Schottky barrier height of Si depending on work function of contact metal. c is the slope of the line. c = 0 line represents the perfect independence of SB height on metal work function, and c = 1 line represents perfect dependence of SB height on metal work function. Adapted from Ref.[12].

1.4 Outline of Thesis

In this thesis, the electrical properties of hydrogen-exposed SWNT are studied. After the introducing the structural, electronic structure of SWNT in chapter 1, the backgrounds on the reported properties of hydrogen-exposed CNT is presented in chapter 2.

In chapter 3, we discuss the electron doping effect of hydrogen exposed individual

SWNT and its networks. Using hexagonal boron nitride (hBN) substrates and the *in-situ* 3-terminal electrical measurements, we can rule out the extrinsic effects caused by oxide substrates or oxygen environments that significantly affect the electronic properties of SWNT. The shifted I_{ds}-V_{gs} curves with respect to the hydrogen exposure time are analyzed to reveal the electron doping effect expected on the graphitic materials exposed to hydrogen. Comparing the SWNT device and graphene device having different curvatures, we study the effect of curved structure on the reaction to hydrogen. Raman spectroscopy and X-ray photoelectron spectroscopy (XPS) were performed to check the formation of C-H bond on the SWNT surface. Electrical measurements on the hydrogen exposed metallic SWNT device was carried out to verify the band gap widening of SWNT by exposure to hydrogen. Finally, the hydrogen exposure process of SWNT network FET is demonstrated to open the possibility of scalable fabrication of electron doping using the technique.

In chapter 4, the metal work function-dependent doping effect on SWNT FET is investigated. To obtain the SWNT FET with higher Schottky barrier for the hole injection, we employ the different contact metal that have lower work function such as Cr replacing the Au electrodes. Eventually, SWNT FET with Ti electrodes is exposed to hydrogen to reveal the possibility of realization of *n*-type SWNT FET.

Bibliography

[1] Moore G E 2006 Cramming more components onto integrated circuits, Reprinted from Electronics, volume 38, number 8, April 19, 1965, pp. 114 ff *IEEE solid-state circuits society newsletter* **11** 33-5

[2] Iijima S 1991 Nature (London) Phys *Sci* **354** 56

[3] Dürkop T, Getty S, Cobas E and Fuhrer M 2004 Extraordinary mobility in semiconducting carbon nanotubes *Nano letters* **4** 35-9

[4] Yao Z, Kane C L and Dekker C 2000 High-field electrical transport in single-wall carbon nanotubes *Physical review letters* **84** 2941

[5] Weitz R T, Zschieschang U, Forment-Aliaga A, Ka¨lblein D, Burghard M, Kern K and Klauk H 2009 Highly reliable carbon nanotube transistors with patterned gates and molecular gate dielectric *Nano letters* **9** 1335-40

[6] Wang L, Meric I, Huang P, Gao Q, Gao Y, Tran H, Taniguchi T, Watanabe K, Campos L and Muller D 2013 One-dimensional electrical contact to a two-dimensional material *Science* **342** 614-7

[7] Ilani S and McEuen P L 2010 Electron transport in carbon nanotubes *Annu. Rev. Condens. Matter Phys.* **1** 1-25

[8] Zhou X 2007 Carbon nanotube transistors, sensors, and beyond

[9] Minot E D 2004 *Tuning the band structure of carbon nanotubes*: Cornell University)

[10] Makarovski A, Zhukov A, Liu J and Finkelstein G 2007 Four-probe measurements of carbon nanotubes with narrow metal contacts *Physical Review B* **76** 161405

[11] Svensson J and Campbell E E 2011 Schottky barriers in carbon nanotube-metal contacts *Journal of applied physics* **110** 16

[12] Sze S M and Ng K K 2006 *Physics of semiconductor devices*: John wiley & sons)

Chapter 2

Backgrounds on hydrogen-exposed SWNTs

2.1 Hydrogen storage

Hydrogen has been regarded as one of the most promising energy carriers with great potential. The carbon-free and clean-burning nature makes it attractive as next generation clean fuel. However, achieving efficient storage technique has been the major obstacle that hinders the commercialization of hydrogen as an energy fuel. After the first report on the hydrogen storage in SWNTs in 1997 [1], the CNT was intensively studied for the storage materials for the hydrogen gas [2-6]. Briefly, there were two main approaches for the hydrogen gas storage.

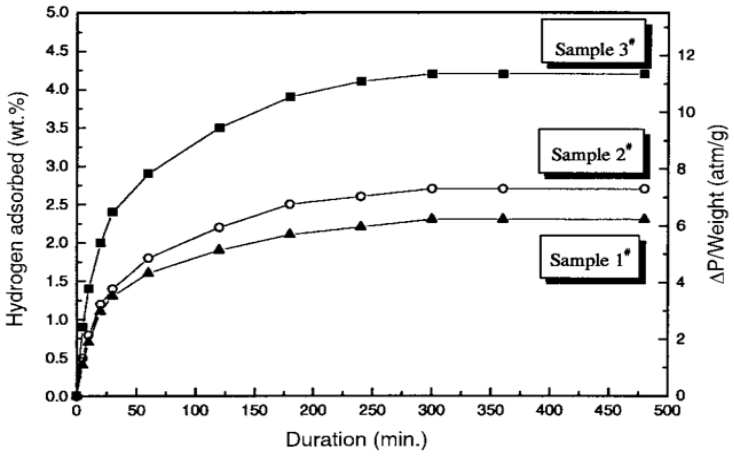

Figure 2.1 Hydrogen storage of CNT. Adapted from Ref. [4].

First, cryo-adsorption technique has been developed for the physisorption of hydrogen gas on the SWNT surface [2]. P. Sudan *et al.* have reported that the molecular hydrogen can be weakly bound to the SWNT surface using van der Waals force [3]. Because the technique relies on the physisorption of hydrogen on the graphitic surface, low temperature is needed to hold the hydrogen gas on the SWNT surface. Maximum ~1 wt% of hydrogen gas can be stored in SWNT surface at ~100 K [3].

Second, hydrogen spillover technique has been performed for the chemisorption of hydrogen on the SWNT surface. Since the dissociation of hydrogen molecule into two hydrogen atoms have a high energy barrier (~3 eV) [7], metal catalysts was employed for the dissociation of hydrogen gas. Metal catalysts such as Pt [5] and Pd [6] were deposited on the SWNT surface to enhance the hydrogen spillover

on SWNT surfaces at room temperature. Because the amount of hydrogen spillover is proportional to the square root of pressure of hydrogen gas [8], this technique requires SWNT to be exposed to high H_2 pressure.

Despite tremendous efforts on the hydrogen storage on CNTs with various approaches [2-6], it is well accepted that CNT-based materials are not suitable for the hydrogen gas storage [9] for two main reasons. First, the recovery rate is low [10]. Second, the capacity is far from the minimum limit of commercial storage requirement for automobiles, 7.5 wt% (suggested by U.S. Department of Energy). Comparing to the compressed gas tank having 13 wt% of storage capacity, the CNT have not showed any promising potentials that alternates the conventional storage techniques.

Carbon material	T (K)	p (MPa)	Hydrogen amount (wt.%)
SWNTs	133	0.04	5–10
SWNTs	80	4–8	8
SWNTs	298	10	4.2
SWNTs	295	0.1067	0.932
SWNTs	77	0.1079	2.37
SWNTs	298	0.1	0.01
SWNTs	77	0.1	1
Li-doped MWNTs	635	–	20
K-doped MWNTs	298	–	14
K-doped MWNTs	–	–	2
CNTs	300	<7	0.5
MWNTs, SWNTs, GNFs	298	7.5	<0.5
MWNTs, SWNTs, GNFs	77	7.5	<1
milled MWNTs	298	8–9	0.66
MWNTs without milling	298	8–9	~0.1
MWNTs milled with MgO	298	8–9	0.69
SWNTs, MWNTs	298	15.2	<1.5
SWNTs, MWNTs	–	<1.48	<1
MWNTs with hydride catalyst	143	7.5	<3.5
CNTs	298	10	2.1
SWNTs	123	2.5	2.4
K-doped SWNTs	33	0.1	2.61
Pt/SWNTs	125	7.8	3.03
Ag/MWNTs	298	2.3	<0.86
MWNTs	77	6.5	<1.21
Pd/MWNTs	77	6.5	0.37
V/MWNTs	77	6.5	0.4
Pd/MWNTs	298	6.5	0.125
V/MWNTs	298	6.5	0.1
BCNTs	300	8	<2
BCNTs	298	8	<2
MWNTs, SWNTs, GNFs	77	7.5	<1
CNTs	–	–	4
MWNTs with transition metals	–	–	8.3
Defective CNTs	573	0.1	1.5

Table 2.1 Experimentally reported hydrogen storage capacities in CNTs. Adapted from Ref.[11].

2.2 Unzipping of SWNT

Because graphene does not have energy band gap [12], making transistor using graphene is difficult. However, the graphene nano-ribbon (GNR) having width less than 50 nm has been suggested for the alternative [13]. Since the charge carriers in GNR have the limited direction as in case of SWNT, it is possible for the GNR to have energy band gap [14].

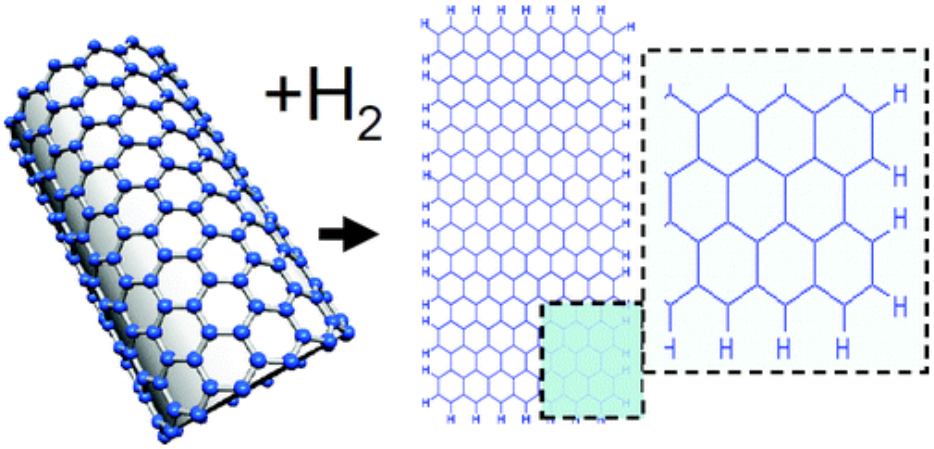

Figure 2.2 Schematic image of GNR made of unzipping of SWNT using hydrogenation. Adapted from Ref.[15].

Unzipping of SWNT has been suggested for the fabrication of GNR [16]. Among the various approaches such as oxidation [17] and acid treatment [18], hydrogenation provides more mild environment less affecting the electronic

structure of SWNT [15]. A. V. Talyzin *et al.* have reported the unzipping effect of SWNT with high-temperature (~400 °C) and high-pressure (~50 bar) environment (Fig. 2.3a) [15]. They observed the spillover effect from Fe catalyst that were used for the synthesis process of SWNT (Figs. 2.3b) [15]. The metallic catalysts used for synthesis of CNT are very difficult to be totally removed. Even after acid purification process, ~1 wt% of metal catalysts such as Fe, Ni are remained [19]. This observation is important because it opens the possibility of spillover effect that is necessary for the chemisorption of hydrogen onto SWNT surface.

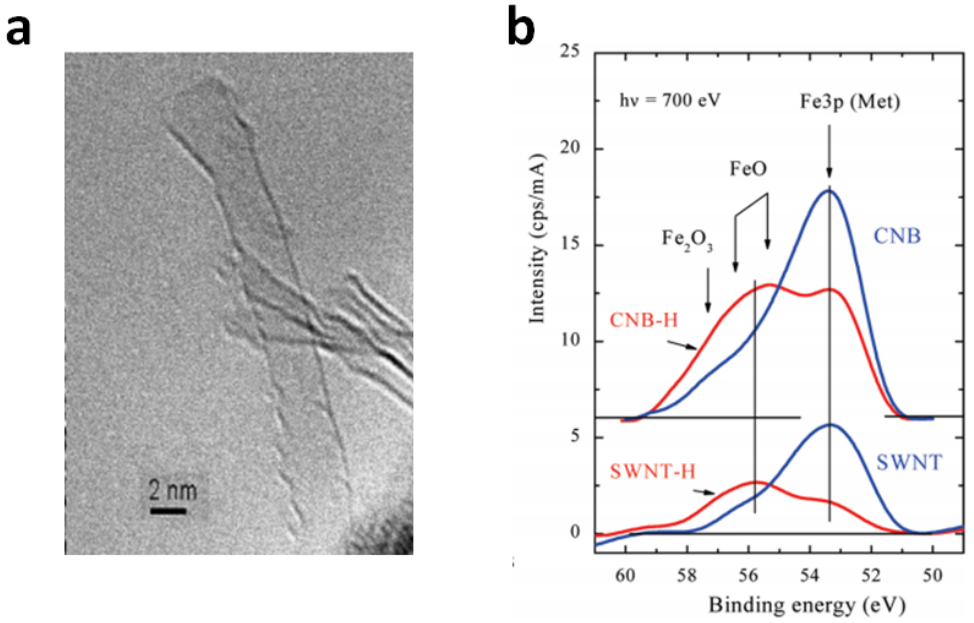

Figure 2.3 Unzipping of SWNT using hydrogen spillover. (a) Transmission electron microscopy of GNR made of unzipping of SWNT *via* hydrogenation. (b) X-ray photoelectron microscopy of SWNT. The Fe is oxidized after hydrogenation

process. It suggests the lowered metal work function during the hydrogen spillover effect. Adapted from Ref.[15].

2.3 Energy band gap widening of hydrogenated SWNT

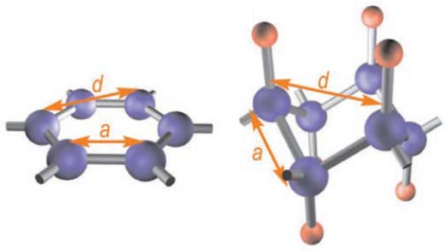

Figure 2.4 Schematic image of graphane. Adapted from Ref.[20].

After the first report on fully hydrogenated graphene, "graphane" [21], the hydrogenation of graphitic layer have attracted attention. The material so called 2-dimensional diamond has been researched for energy band gap opening, and realization of two-dimensional insulating layers. However, making perfect graphane is very difficult because functionalization of dense hydrogen both side of graphene (Fig. 2.4) is challenging [22]. On the other hand, in terms of band gap opening, several successful outputs on the hydrogenation of metallic SWNT have been reported. K. S. Kim *et al.* have reported that energy band structure of

hydrogenated metallic SWNT calculated by density functional theory (DFT) shows the opening the energy band gap [23]. Also, they experimentally observed the semiconducting behavior of SWNT after hydrogen molecule exposure process [24]. Moreover, G. Zhang *et al.* have reported the similar result, increased on-off ratio of metallic SWNT after hydrogen plasma treatment [25].

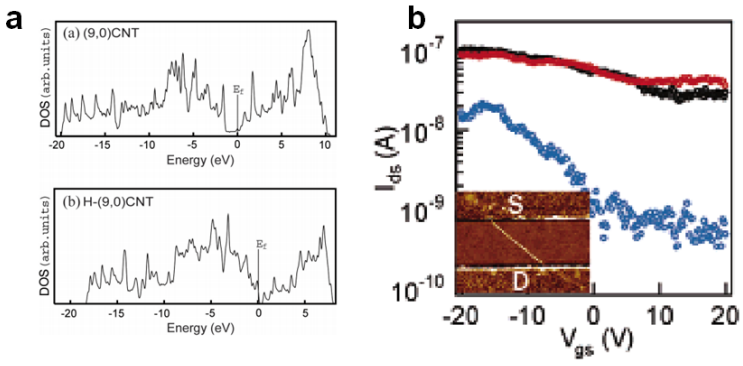

Figure 2.5 Band gap widening of SWNT. (a) Density of state (DOS) of pristine SWNT and hydrogenated SWNT calculated by DFT. Adapted from Ref. [23]. (b) I_{ds}-V_{gs} curves of metallic SWNT (black) before and (red) after hydrogenation. Adapted from Ref.[25].

It is well accepted that formation of C-H bond induces the band gap widening effects. There are several options to identify the successful hydrogenation of SWNT. XPS is one of the mostly used techniques for characterization of C-H bond on the graphitic surface. As mentioned in Chapter 1, SWNT is a rolled graphene

strap and graphene lattice consists of carbon atoms with sp^2 hybridization. If the SWNT is functionalized, the π electron makes covalent bond with hydrogen resulting in sp^3 hybridization of carbon. It was reported that the sp^3 hybridization have ~0.8 eV larger energy than sp^2 hybridization [26]. As shown in Fig. 2.6a, this energy difference can be detected by photoelectron generated by X-ray irradiation.

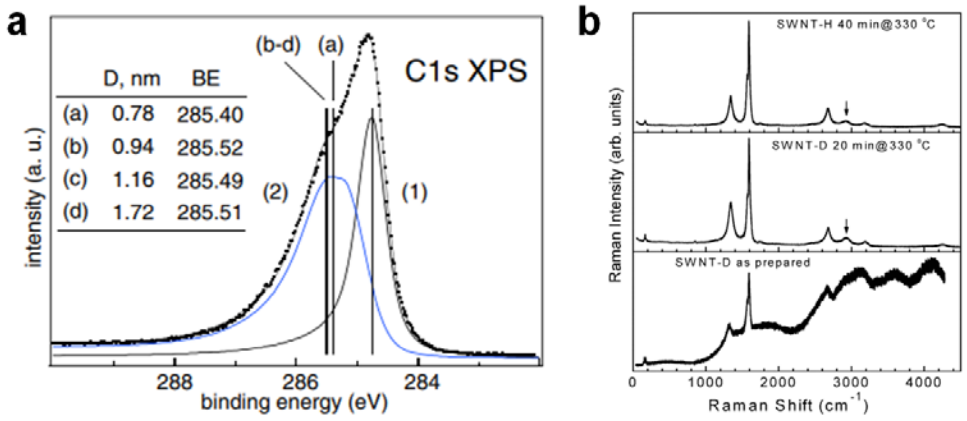

Figure 2.6 Characterization tools for hydrogenated SWNT. (a) C1s profile of XPS. Blue line represents the sp^3 peak of SWNT generated by hydrogen exposure process. The additional broad peak at the lower energy is occurred. Adapted from Ref. [26]. (b) From bottom to top, Raman spectra of chemically hydrogenated SWNT, 20 min annealed SWNT and 40 min annealed SWNT are presented. Adapted from Ref. [27].

Raman spectroscopy is used to get the information of phonon modes in the

SWNT lattices. Figure 2.6b shows the Raman spectra of as prepared hydrogenated SWNT, 20 min annealed SWNT and 40 min annealed SWNT. The two most intense peak in the spectra of Fig. 2.6b are *D* mode (left) and *G* mode (right). *G* mode at ~1592 cm^{-1} is graphitic mode used to be seen in graphene based structures and *D* mode at ~1350 cm^{-1} is detected in disordered graphitic lattice [28]. So, the ratio of *G* mode and *D* mode are used for the quantitative characterization of disorders on SWNT [28]. Normally, the *D* and *G* modes do not interact with each other because it is forbidden process [28]. However, with scattering sites on the SWNT surface such as C-H bond, the second order combination mode of $D + G$ (at ~2930 cm^{-1}) arises [28]. As C-H bond acts as a medium, two different phonons (*D* and *G* mode) of SWNT can be combined [27, 29]. So that, the $D + G$ mode is regarded as a one of the important fingerprints of successful functionalization of SWNT.

Bibliography

[1] Dillon A C, Jones K, Bekkedahl T, Kiang C, Bethune D and Heben M 1997 Storage of hydrogen in single-walled carbon nanotubes *Nature* **386** 377-9

[2] Ye Y, Ahn C, Witham C, Fultz B, Liu J, Rinzler A, Colbert D, Smith K and Smalley R 1999 Hydrogen adsorption and cohesive energy of single-walled carbon nanotubes *Applied Physics Letters* **74** 2307-9

[3] Sudan P, Züttel A, Mauron P, Emmenegger C, Wenger P and Schlapbach L 2003 Physisorption of hydrogen in single-walled carbon nanotubes *Carbon* **41** 2377-83

[4] Liu C, Fan Y, Liu M, Cong H, Cheng H and Dresselhaus M S 1999 Hydrogen storage in single-walled carbon nanotubes at room temperature *Science* **286** 1127-9

[5] Reddy A L M and Ramaprabhu S 2008 Hydrogen adsorption properties of single-walled carbon nanotube—Nanocrystalline platinum composites *International journal of hydrogen energy* **33** 1028-34

[6] Suttisawat Y, Rangsunvigit P, Kitiyanan B, Williams M, Ndungu P, Lototskyy M, Nechaev A, Linkov V and Kulprathipanja S 2009 Investigation of hydrogen storage capacity of multi-walled carbon nanotubes deposited with Pd or V *International journal of hydrogen energy* **34** 6669-75

[7] Tada K, Furuya S and Watanabe K 2001 Ab initio study of hydrogen adsorption to single-walled carbon nanotubes *Physical Review B* **63** 155405

[8] Cheng H, Chen L, Cooper A C, Sha X and Pez G P 2008 Hydrogen spillover in the context of hydrogen storage using solid-state materials *Energy & Environmental Science* **1** 338-54

[9] Darkrim F L, Malbrunot P and Tartaglia G 2002 Review of hydrogen storage by adsorption in carbon nanotubes *International journal of hydrogen energy* **27** 193-202

[10] Ong Y T, Ahmad A L, Zein S H S and Tan S H 2010 A review on carbon nanotubes in an environmental protection and green engineering perspective *Brazilian Journal of Chemical Engineering* **27** 227-42

[11] Oriňáková R and Oriňák A 2011 Recent applications of carbon nanotubes in hydrogen production and storage *Fuel* **90** 3123-40

[12] Ilani S and McEuen P L 2010 Electron transport in carbon nanotubes *Annu. Rev. Condens. Matter Phys.* **1** 1-25

[13] Fujita M, Wakabayashi K, Nakada K and Kusakabe K 1996 Peculiar

localized state at zigzag graphite edge *Journal of the Physical Society of Japan* **65** 1920-3

[14] Huang L F, Zhang G R, Zheng X H, Gong P L, Cao T F and Zeng Z 2013 Understanding and tuning the quantum-confinement effect and edge magnetism in zigzag graphene nanoribbon *Journal of Physics: Condensed Matter* **25** 055304

[15] Talyzin A V, Luzan S, Anoshkin I V, Nasibulin A G, Jiang H, Kauppinen E I, Mikoushkin V M, Shnitov V V, Marchenko D E and Noreus D 2011 Hydrogenation, purification, and unzipping of carbon nanotubes by reaction with molecular hydrogen: road to graphane nanoribbons *ACS nano* **5** 5132-40

[16] Brumfiel G 2009 Nanotubes cut to ribbons new techniques open up carbon tubes to create ribbons *Nature*

[17] Sinitskii A, Fursina A A, Kosynkin D V, Higginbotham A L, Natelson D and Tour J M 2009 Electronic transport in monolayer graphene nanoribbons produced by chemical unzipping of carbon nanotubes *Applied Physics Letters* **95** 253108

[18] Kosynkin D V, Higginbotham A L, Sinitskii A, Lomeda J R, Dimiev A, Price B K and Tour J M 2009 Longitudinal unzipping of carbon nanotubes to form graphene nanoribbons *Nature* **458** 872-6

[19] García-García F, Pérez-Cabero M, Nevskaia D, Rodríguez-Ramos I and Guerrero-Ruiz A 2008 Improving the synthesis of high purity carbon nanotubes in a catalytic fluidized bed reactor and their comparative test for hydrogen adsorption capacity *Catalysis today* **133** 815-21

[20] Elias D C, Nair R R, Mohiuddin T, Morozov S, Blake P, Halsall M, Ferrari A C, Boukhvalov D, Katsnelson M and Geim A 2009 Control of graphene's properties by reversible hydrogenation: evidence for graphane *Science* **323** 610-3

[21] Sluiter M H and Kawazoe Y 2003 Cluster expansion method for adsorption: Application to hydrogen chemisorption on graphene *Physical Review B* **68** 085410

[22] Sofo J O, Chaudhari A S and Barber G D 2007 Graphane: A two-dimensional hydrocarbon *Physical Review B* **75** 153401

[23] Kim K S, Park K A, Kim H J, Bae D J, Lim S C, Lee Y H, Kim J R, Kim J-J and Choi W B 2003 Band gap modulation of a carbon nanotube by hydrogen functionalization *JOURNAL-KOREAN PHYSICAL SOCIETY* **42** S137-42

[24] Kim K S, Bae D J, Kim J R, Park K A, Lim S C, Kim J J, Choi W B, Park C Y and Lee Y H 2002 Modification of electronic structures of a carbon nanotube by hydrogen functionalization *Advanced Materials* **14** 1818-21

[25] Zhang G, Qi P, Wang X, Lu Y, Mann D, Li X and Dai H 2006 Hydrogenation and hydrocarbonation and etching of single-walled carbon nanotubes *Journal of the American Chemical Society* **128**

6026-7
[26] Nikitin A, Ogasawara H, Mann D, Denecke R, Zhang Z, Dai H, Cho K and Nilsson A 2005 Hydrogenation of single-walled carbon nanotubes *Physical review letters* **95** 225507
[27] Meletov K, Bashkin I, Shestakov V, Krestinin A, Davydov V, Pulikkathara M, Khabashesku V, Arvanitidis J, Christofilos D and Kourouklis G 2008 Raman study of hydrogenated and fluorinated single-walled carbon nanotubes *Fullerenes, Nanotubes and Carbon Nanostructures* **16** 322-9
[28] Dresselhaus M S, Jorio A, Hofmann M, Dresselhaus G and Saito R 2010 Perspectives on carbon nanotubes and graphene Raman spectroscopy *Nano letters* **10** 751-8
[29] Meletov K, Maksimov A, Tartakovskii I, Bashkin I, Shestakov V, Krestinin A, Shulga Y M, Andrikopoulos K, Arvanitidis J and Christofilos D 2007 Raman study of the high-pressure hydrogenated single-wall carbon nanotubes: In search of chemically bonded and adsorbed molecular hydrogen *Chemical physics letters* **433** 335-9

Chapter 3

SWNT field-effect transistor (FET) exposed to hydrogen

3.1 Introduction

3.1.1 Electron doping effect of hydrogenated graphitic materials

J. A. Vergens *et al.* have reported that hydrogen's electron affinity dominates the energetic balance in the charged systems and the extra electron is predominantly attracted to a region nearby the chemisorbed atom [1]. B. R. Matis *et al.* calculated the increased work function of graphitic layer after hydrogenation suggesting that electron doping effect on the system [2]. There are more works reporting the electron doping effect of hydrogenated graphitic layer in theoretical [3, 4] and experimental [5, 6] point of views.

One of the huge obstacles for observing the electron doping effect on graphitic layers *via* electrical measurements is extrinsic effects from environmental

conditions, *i.e.* ambient air. As a strong hole type dopant [7], oxygen hinders electrical measurements on the electron doping effect caused by hydrogenation. Thus, *in-situ* electrical measurements are necessary to rule out the extrinsic effects from oxygen; it allows observing intrinsic properties caused by hydrogenation of graphitic layers. The left-shifted charge neutrality point (CNP) on I_{ds}-V_{gs} curve has been consistently observed in the *in-situ* measurements of hydrogenated graphitic layers [5, 8, 9]. The reason why left-shifted CNP strongly suggest electron doping on graphitic layers is following. To reach the CNP of graphene in the plane capacitor model, significant magnitude of negative gate voltage is needed to induce more positive charge on the graphene plate to compensate electron doping effect. Moreover, left-shifted gate dependence of thermoelectric power [10] and red-shifted *G* and *2D* mode in Raman spectroscopy [11] were observed in the hydrogenated graphitic layers supporting that the electron doping effect followed by hydrogenation of graphitic layers. Not only electron doping effect but also short-range scattering was observed in hydrogenated graphitic layers [12]. The observations suggest the formation of C-H covalent bond generating more scattering sites on the surface [12]. The formation of covalent bond is in consistent with the other observations such as TEM [8], Raman spectroscopy [5], and electrical measurement under vacuum [11]. The competition between electron doping induced carrier density enhancement and C-H bond induced short-range scattering was observed in the hydrogenated graphitic layers [12]. The effects from two different mechanisms result in the final electrical properties of hydrogenated graphitic layers [12].

SWNT is regarded as a cylindrical shape of graphene. It has been reported that the curvature of surface of CNT caused by cylindrical shape lowers the activation energy of functionalization of SWNT surface [13, 14]. As fictionalization of graphitic surface accompanies the structural change with increased strain, the originally curved SWNT structure is advantages on the hydrogenation [13]. Zhang *et al.* has reported that the nanotubes with smaller diameter have higher reactivity with hydrogen atoms [14]. Considering CNTs have higher responsibility with hydrogen due to its curved structure, it is expected that CNTs show similar response with graphene (*i.e.* electron doping effect) with hydrogen exposure process.

3.1.2 Motivation of SWNT exposure to hydrogen

However, it is very hard to observe the intrinsic electronic properties of hydrogenated carbon nanotubes. It is reported that the CNT channel area [15] and contact area (Schottky barrier) [16] of carbon nanotubes are very sensitive to environments, particularly to oxygen. Therefore, *in-situ* electrical measurement is necessary for the experimental observation of doping effect *via* hydrogen exposure on SWNT FET devices. However, *in-situ* electrical measurement with hydrogen exposure processes is very challenging because hydrogenation process accompanies harsh condition for electrical measurements [14, 17]. Despite the difficulty of performing experiments, the electron doping effect on SWNT should be useful for applications. Because graphene-based electronic devices usually have

p-type electrical properties [7, 16], development of *n*-type device has been desired for the composition of complete logic circuit in the next generation electronics.

Here we report the electron doping effect of SWNT caused by hydrogen exposure process. *In-situ* 3-terminal electrical measurements were used to observe the intrinsic electronic properties of hydrogen-exposed SWNT. Kelvin probe force microscopy (KPFM) was performed to the SWNTs on Si substrate to verify the electron doping effect by changed surface potential. The shift of time-dependent I_{ds}-V_{gs} curve was continuously monitored throughout the hydrogen exposure process. Comparing the electrical data of SWNT device to the planar graphene sheet device, the effect of the curved structure of SWNT in the electrical property was investigated. Raman spectroscopy and XPS were conducted on the SWNTs to check the formation of C-H covalent bond on the surface of SWNTs. Metallic SWNT device were exposed to hydrogen molecules to observe the modulation of electronic property due to the C-H bond formation. Finally, this behavior was also observed in the random network SWNT FET with the commercial SiO_2/Si substrate, which showed the possibility of scalable fabrication of electron doping on the SWNT using hydrogen exposure process.

3.2 Experimental

To reduce the extrinsic effect from oxide substrates [18], few layer hBN was used for the substrate of SWNT FETs. Few-layer hBN flake was exfoliated on the SiO_2

(285nm)/highly *p*-doped Si substrate. The substrate was spin-coated by PMMA A4 with 3000 rpm for 60 s. Using the field emission scanning electron microscope (FE-SEM), electron beam lithography was performed to draw the shape of electrodes. After development using MIBK/IPA 1:3 solution, 5 nm Ti / 30 nm Au was deposited. Lift off process was followed using acetone/IPA leaving the Au electrodes on the hBN substrate. We performed dielectrophoresis (DEP) using 99 % semiconducting single-walled carbon nanotube solution (IsoNanotubes-S, Nanointegris) with concentration of 100 ng/ml. Figure 3.1 shows the DEP technique we applied in this experiment. ~1 V of AC voltage with ~1 MHz frequency was applied to the ~2 μm apart electrodes for several seconds. Then, we checked electrically if the SWNTs were contacted between the electrodes. We repeated this process until we get the electrical signal. Because metallic SWNT is much more sensitive to the AC voltage applied to electrode than semiconducting SWNT [10], the probability of making metallic SWNT FET was not that low even using the 99% semiconducting enriched SWNT solution. Therefore, both metallic and semiconducting SWNT devices used in this chapter could be obtained by this single technique. Once we sense the electrical signal from SWNTs, the device was mounted to the high-pressure, high-temperature chamber that allows *in-situ* electrical measurements. After 10 h of degassing process at 400 K under ~$2 \cdot 10^{-6}$ torr of dynamic vacuum condition, hydrogen pressure of 20 bar was injected to the chamber. The whole hydrogen exposure process was monitored using 3-terminal electrical measurements by Keithley 4200 semiconductor characterization system. In other words, drain-source current at the fixed drain-source voltage (0.1 V)

depending on gate-source voltage sweep from +50 V to -50 V was performed every 15 min ~ 30 min for total 15 h of hydrogen exposure process.

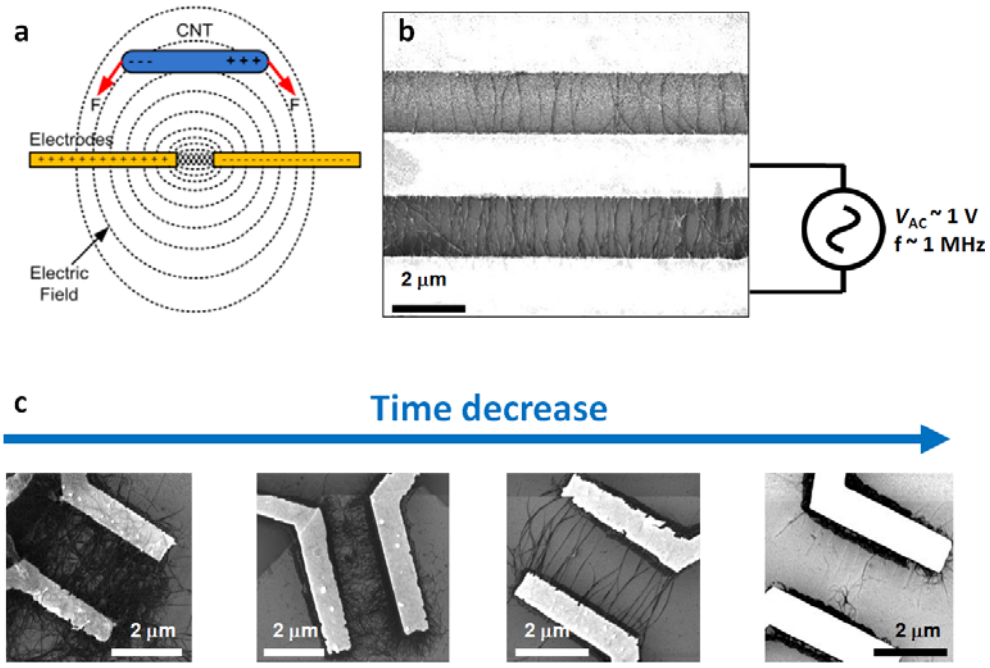

Figure 3.1 DEP of SWNT. (a) Schematic image of DEP on CNTs. Image is adapted from Ref.[19]. (b) SEM image of SWNT array made by DEP. (c) Example SEM images of SWNTs on hBN made by DEP technique. The density of SWNT decreases as AC voltage applied time decreases.

For the XPS and Raman spectroscopy, SWNT film (IsoNanotubes-S, Nanointegris) was degassed in the same chamber with same condition before the first measurement. X-ray with ~1490 eV energy from Al source (K_α) was used for the characterization. The photoelectron was detected under 2.2×10^{-9} Torr condition.

The Raman spectroscopy was performed on the same sample under ambient condition with excitation by 532 nm laser. After hydrogen exposure process at 400 K in 20 bar pressure of H_2 gas for 24 h, the XPS and Raman spectroscopy were followed with the measurement conditions described above.

3.3 Results and discussion

3.3.1 *In-situ* electrical measurements of hydrogen-exposed SWNT

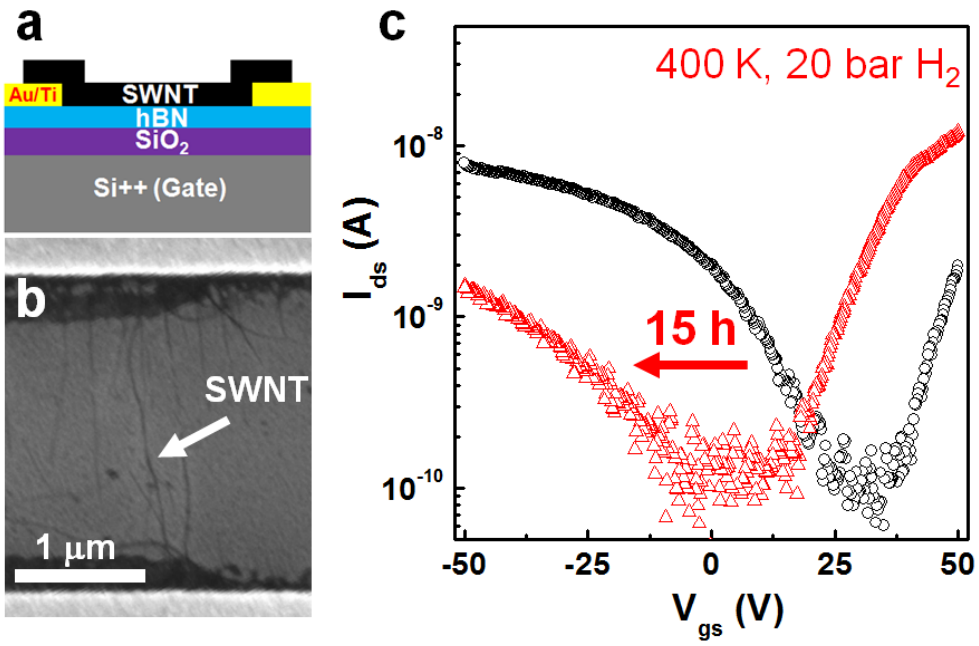

Figure 3.2 *In-situ* 3-terminal electrical measurements of SWNT device with hydrogen exposure process. (a) Schematic image of cross-sectional view of SWNT

FET. Semiconducting SWNT was deposited onto the pre-patterned gold electrodes on hBN/SiO_2 substrate by DEP technique. The final device becomes 3-terminal field-effective transistor (FET). (b) The top view of the device obtained by SEM. (c) I_{ds}-V_{gs} curves (black circles) before and (red triangles) after hydrogen exposure of the SWNT FET.

Figure 3.2a shows the schematic of cross-sectional view of the semiconducting SWNT device. DEP was used to obtain the bottom contacted device. Although DEP provides high selectivity on metallic SWNTs [20], we often obtained semiconducting SWNTs using the semiconducting SWNT rich solution (99%) [21]. The deposited SWNT was cleaned by DI water and IPA, and then it was mounted to the high-pressure electrical measurement chamber.

After degassing for 10 h at 400K, the I_{ds}-V_{gs} with fixed V_{ds} (to 0.1 V) was measured as presented by black curve in Figure 3.2c. The device clearly shows ambipolar nature of SWNT. We defined the minimum current (around ~150 pA) are as off-state regime. The hole-type conduction is shown at the left side of off-state regime as negative gate voltage applied to highly doped Si bottom gate induces hole-type charge carriers on the SWNT surface. On the other hand, the positive voltage to Si bottom gate induces electrons on the SWNT surface making the electrons to majority charge carrier at the regime.

After 15 h of highly pure hydrogen (99.9999%) exposure process with 400 K and 20 bar, the device obviously shows left-shifted I_{ds}-V_{gs} curve as presented in red

triangles of Fig. 3.2c. The left-shift in I_{ds}-V_{gs} curve suggest increased Fermi level of SWNT channel, *i.e.* electron doping of SWNT [22]. As electron is doped to the SWNT channel, more negative gate voltage is needed to reproduce the same I_{ds}-V_{gs} curve. The left-shifted I_{ds}-V_{gs} curve has also been reported on the K-doped SWNT FET where K is a strong electron donor [23]. The Schottky barrier height change can be detected by asymmetrically changed sub-threshold slopes in the I_{ds}-V_{gs} curves [22]. The shifted curve effect is clearly distinguished from the changed Schottky barrier height effect that originates the changed work function of contact metals. More discussion on the contact area (Schottky barrier) is available in chapter 4.

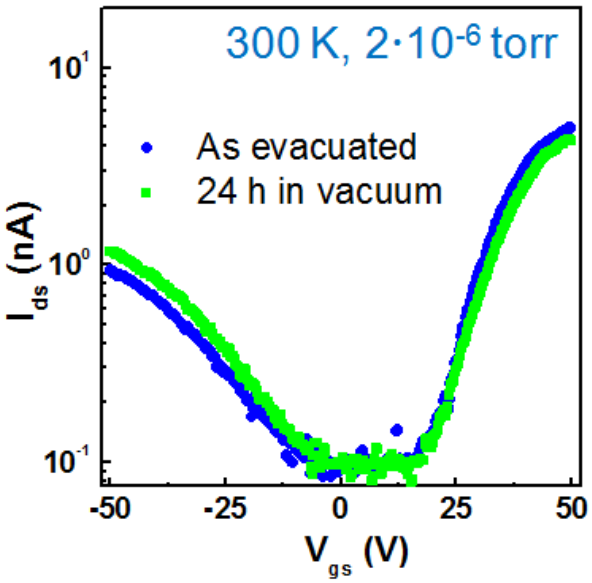

Figure 3.3 Stability of the electron doping effect. The shifted I_{ds}-V_{gs} curve was nearly maintained under dynamic vacuum condision (~2·10^{-6} torr) for 24 h at the

room temperature.

Figure 3.3 shows the stability of hydrogen-exposed SWNT device in a vacuum. After the hydrogen exposure process, the device was cooled down to room temperature. then, we quickly evacuated the chamber from 20 bar of hydrogen to $2 \cdot 10^{-6}$ torr. The blue dots in Fig. 3.3 represent the I_{ds}-V_{gs} curves of the SWNT FET just after the evacuation. We observed the relatively *n*-type electrical property due to H_2 exposure (corresponding to the shifted I_{ds}-V_{gs} curves due to the electron doping effect) is maintained even after the evacuation process for 24 h (green dots). Therefore, physisorption on SWNT surface can be ruled out. If the change in electrical properties due to hydrogen exposure originates from physisorption of hydrogen molecules, the change should disappears when the hydrogen chamber is evacuated. However, the shifted I_{ds}-V_{gs} curve was maintained even after the SWNT was totally under vacuum condition. This result strongly suggests the electron doping effect does not come from the physisoprion of hydrogen molecule on SWNT surface. Also, our observation is in aggrement with the previous theoretical study showing that the absense of charge transfer between hydrogen molecules and graphitic surface in case of physisorption [24]. Consequently, the significant change in the electronic structure is possibly attributed to the formation of covalent bond of carbon and hydrogen atoms through chemisorption as reported in graphene cases [3, 5, 10]. More characterizations on the C-H bond are discussed in section 3.3.5.

3.3.2 Surface potential spectroscopy of hydrogen-exposed SWNTs

Kelvin probe force microscopy (KPFM) is performed to check the change of surface potential after hydrogen exposure process. Using the AC and DC voltage applied metallic cantilever mounted on AFM, the capacitance between metal-coated AFM tip and sample surface is monitored. Since the DC voltage making the system equillibrium are recorded with the positional information of the tip [25], we can obtain the information of surface potential. The surface potential maps of the sample with AFM images are shown in Fig. 3.4.

Thin SWNT network on Si substrate are compared before and after hydrogen exposure process. Because Si does not react with hydrogen gas [26], the difference of potential between SWNTs and Si background was analysed. Figures 3.4a,b are AFM images of network SWNT film on Si substrate. The two different region of one sample shows similar height of SWNT film. Figures 3.4c,d show the decreased surface potential after hydrogen exposure. The decreased surface potential suggests electron dopping effect on SWNT [25]. Once the electron is doped to SWNTs, SWNT contains more electrons. That is why more negative DC voltage is needed to be applied to the metallic AFM tip to compensate the electron doping effect making the system equillibrium [25]. The result supports the electron doping effect on SWNT observed by the electrical transport experiments in Fig. 3.2.

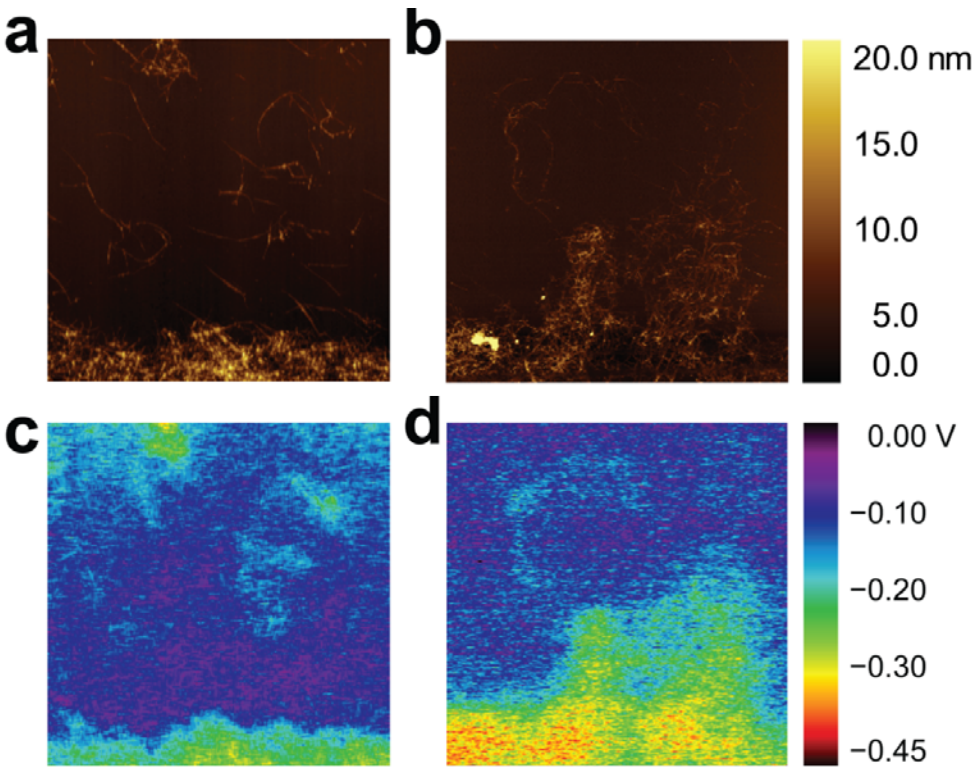

Figure 3.4 Surface potential microscopy on SWNTs with hydrogen exposure. The AFM image of SWNT network on Si substrate before (a) and after (b) hydrogen exposure. KPFM of the network before (c) and after (d) hydrogen exposure. Adapted from Ref.[27].

3.3.3 Exposure time-dependent electrical property

The custom-made *in-situ* electrical measurement system enables the contiuous monitoring of I_{ds}-V_{gs} curve without interruption from extrinsic conditions such as

oxygen and waters that significantly affect the electronic properties of SWNTs. Figure 3.5 shows the color map of I_{ds}-V_{gs} curve measured during the hydrogen exposure process. As described in Fig. 3.2c black circles, the pristine state at time 0 h shows more red colored area at upper side of the map, *i.e*. negative gate voltage side of the curves. As mentioned above, the upper side represents hole-type conduction of SWNT. As the curve shifts, the red zone of upper side become smaller while the red zone of down side is expanded. The red zone of upper side disappears faster than the expansion of red zone of down side due to the asymetric changes of Schottky barriers. The details on the effect from Schottky barrier will be disscussed in chapter 4. Because the red zone of bottom side represents the electron type conduction, this change clearly shows the smooth transition of majority carrier from hole to electron.

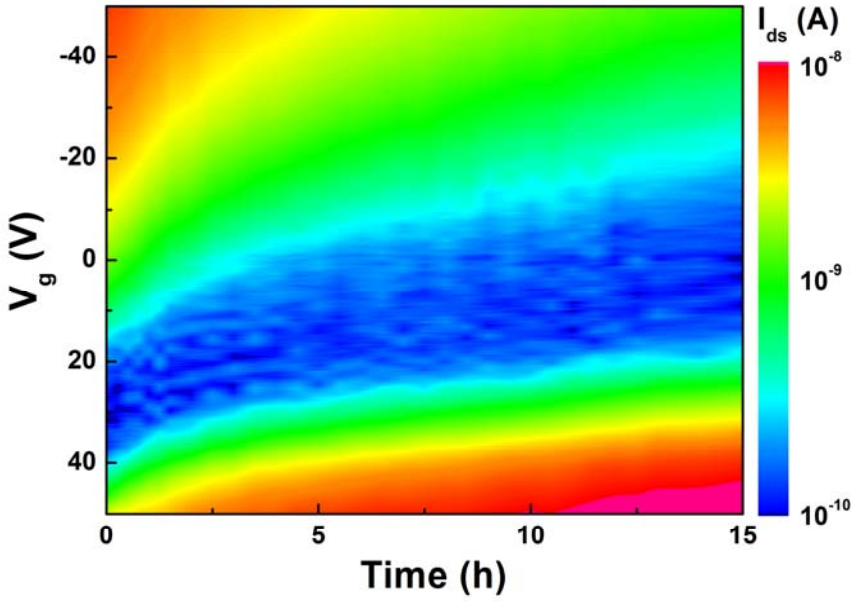

Figure 3.5 Time dependence of hydrogen exposure on SWNT. Color map of *in-situ* electrical measurements of SWNT during high-pressure (20 bar), high-temperature (400 K) hydrogen exposure process.

Blue color represents the minimum conduction of the device. The width of the minimum conduction regime clearly increses as exposure time increases. We define the difference of gate voltage having the current of ~200 pA in the I_{ds}-V_{gs} curve as off-state width (ΔV_{off}). The widened ΔV_{off} according to the increased hydrogen exposure time is observed. This widening is possibly attributed to the electronic band structure changed by C-H bond formation on SWNT surface. Kim *et al.* have reported that DFT calculation on SWNT with C-H bond shows change in energy band structure with energy band gap widening [28]. More detailes of the off-state widening effect will be discussed in section 3.3.6.

3.3.4 Effect of curved structure

To investigate the effect of curved structure on the reaction with hydrogen, we compared the time-dependent shift of I_{ds}-V_{gs} curves of graphene and SWNT under 20 bar of hydrogen gas exposure. Figure 3.6 shows *in-situ* electrical measurements during hydrogen gas exposure of graphitic structures with different curvatures. Black circles of Fig. 3.6b is the I_{ds}-V_{gs} curve of mechanically exfoliated single-layer graphene device after 10 h of degassing process. The energy band structure of

graphene has linear dispersion near the Fermi level of K-point. Also, the density of states (DOS) of graphene has linear dependance according to its energy level as depected in inset of Fig. 3.6b. The conduction band and valence band meet at the CNP. The CNP is also called as "Dirac point", because charge carrier at this regime acts as a massless fermion (Dirac fermion) (the mass of charge carrier is inversly proportional to the curvature of energy band structure.) [29]. In accordance with DOS, the I_{ds}-V_{gs} curve of graphene device shows highly symmetrical shape. The minimum current represents Dirac point where the DOS of graphene have minimum value (ideally zero). We define the gate voltage that the Fermi level of graphene is located at the Dirac point as Dirac voltage, V_D. So, the V_D is represented as the gate voltage corresponding to the minimum current value of the I_{ds}-V_{gs} curve.

After 15 h of hydrogen exposure process, the V_D is left-shifted with the I_{ds}-V_{gs} curve of graphene as depicted with red triangles of Fig. 3.6b. It is note worthy that the left-shifted V_D corresponds to the electron doping of the structure [5, 8, 9]. If graphene is doped by electron, high negative gate voltage is needed to reach the CNP. In other words, doped electrons can be compensated by the increased hole carriers induced by negative gate voltage. Therefore, the ~18 V left-shifted V_D after hydrogen exposure process shows the electron doping on graphene.

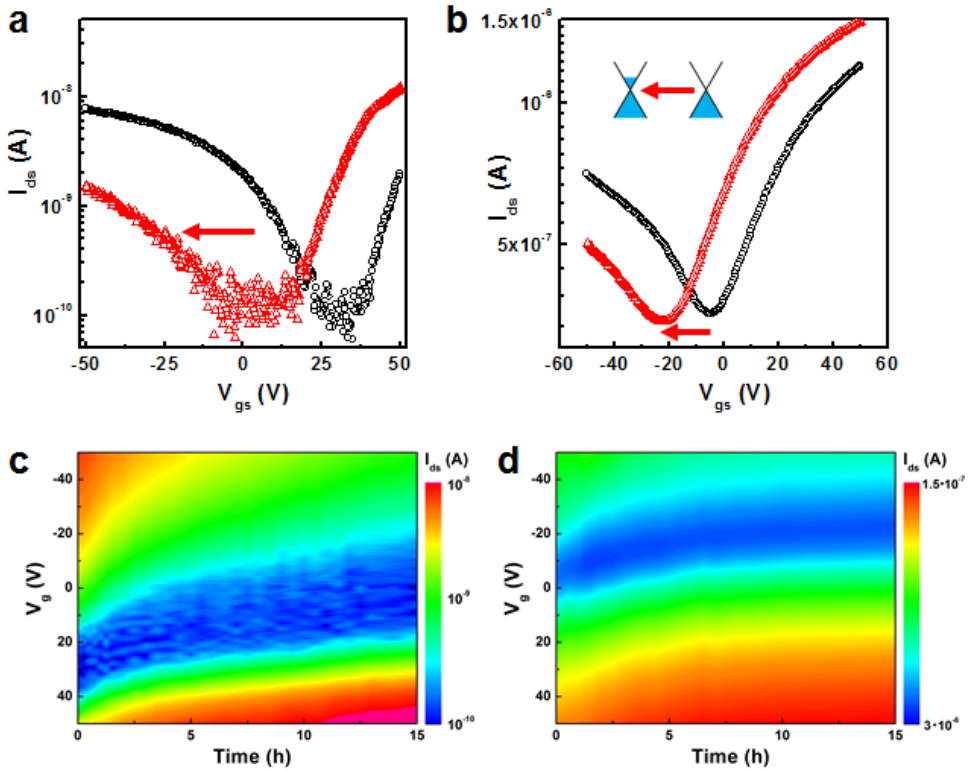

Figure 3.6 *In-situ* electrical measurements during hydrogen exposure of graphitic structures with different curvatures. I_{ds}-V_{gs} curves of pristine (black circles) and hydrogen-exposed (red triangles) (a) SWNT and (b) graphene device. I_{ds}-V_{gs} curves of (c) SWNT and (d) graphene devices shift during hydrogen exposure process. Both hydrogen exposure process were perfomed using 400 K, 20 bar of hydrogen gas. V_{ds} for graphene device is fixed to 1 mV.

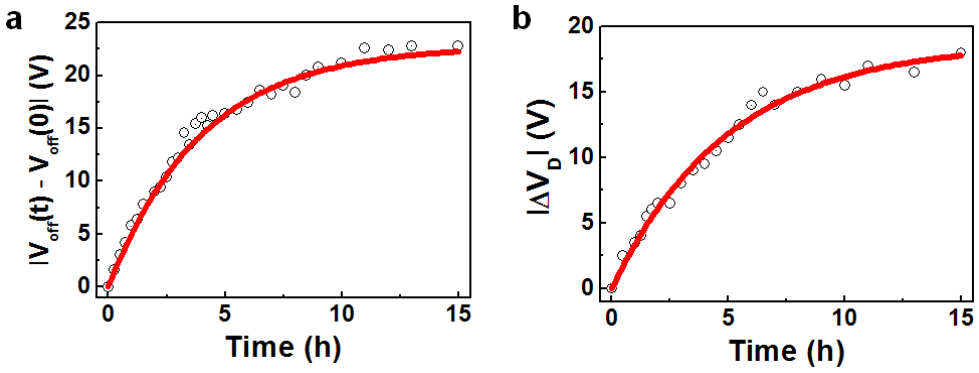

Figure 3.7 Hydrogen exposure time-dependent I_{ds}-V_{gs} curve shift of graphitic layers with different curvatures. (a) Time dependence of shifted off-state voltage (V_{off}(t)) of SWNT device. The V_{off}(t) is defined as the gate voltage where the drain-source current of electron type carrier becomes below $2 \cdot 10^{-11}$ A. (b) Time dependence of shifted Dirac voltage, V_D of graphene.

Figure 3.7 shows hydrogen exposure time dependence of I_{ds}-V_{gs} curve shift of graphitic layers with different curvatures. For the quantative analysis of SWNT device, V_{off}(t) is defined as the gate voltage where the drain-source current of electron type carrier becomes below $2 \cdot 10^{-11}$ A. V_D is used for the analysis of graphene device. The data are presented as black empty circles.

It is well accepted that the hydrogenation of graphitic materials is exponentially dependent on the exposure time [5, 30-32]. To analyse the time-dependent reaction of hydrogen on graphitic layers, we used a simplified model as described below [12, 30]. First of all, we assume that there are limited number of sites (N) where can be occupied. All of the unoccupied sites are energetically equivalent and the occupied

sites are immobile states. Interections between occupied sites are ignored in this model. The summation of number of unoccupied sites (U(t)) and occupied sites (O(t)) are equal to the number of saturated sites (N_{sat}(t)).

$$U(t) + O(t) = N_{sat}$$

We also assume that the process occurrs totally matching responce (one atom occupies one site) as expected in hydrogenation of graphitic materials. And the reaction rate is proportional to the number of unoccupied sites, U(t). Therefore, the speed of responce can be described as,

$$\frac{dO(t)}{dt} = -\frac{dU(t)}{dt} = -kU(t),$$

where the reaction constant k shows the responce speed and the inverse of k, τ, represents the responce time. From the differential equation, we obtained

$$O(t) = ae^{-kt} + b.$$

From the boundary condition at $t = 0$ and $t \to \infty$, we obtain $b = -a$ and $a = N_{sat}$. So, the equation becomes

$$O(t) = N_{sat}(1 - e^{-kt}).$$

Because the number of ocupied sites are proportional to the shifted I_{ds}-V_{gs} curves, we can use the equation for the both SWNT and graphene device with simple mathmatical works [12, 27]. The fitting curves obtained from the model are

presented as red lines in Fig. 3.7. Both curves show ~0.99 adj-R^2 values. The adj-R^2 is a modification of R^2 that adjusts for the number of explanatory terms in a model relative to the number of data points. So, the adj-R^2 near to 1 represents the good correspondence of the model and measured values.

We obtained $\Delta V_{off}^{Sat} = 22.7$ and $k_1 = 0.251$ as fitting parameters of SWNT device (Fig. 3.7a). $\Delta V_{off}^{Sat} = 18.7$ and $k_1 = 0.200$ are obtained from the graphene device (Fig. 3.7b). We found that SWNT has higher ΔV_{off}^{Sat} and k values compared with those of graphene. The higher *k* value may be attributed to the lower activation energy related to the formation of C-H bonds. It has been reported that the curvature of CNT caused by cylindrical shape lowers the activation energy for functionalization [13, 14]. Functionalization of graphene layers should accompany the structural change of graphene lattice. Park *et al.* defined pyramidal angle θ_p for the quantitative analysis of the structural change of graphene lattice [13]. In the most of functionalization processes, the ground state of final output has larger pyramidal angle because it lowers the total energy of the system [13]. In the curved structure such as carbon nanotubes, the pyramidal angle is already larger than planar graphene sheet and this is advantageous to the functionalization on graphene surface because of lowered activation energy [13]. This result was also proved experimentally. Zhang *et al.* has reported that the nanotubes with smaller diameter have higher reactivity with hydrogen atoms [14]. In this point of view, we confirmed that the curved graphitic structure enhances reaction of hydrogen molecules.

3.3.5 Raman spectroscopy and XPS of hydrogen-exposed SWNT

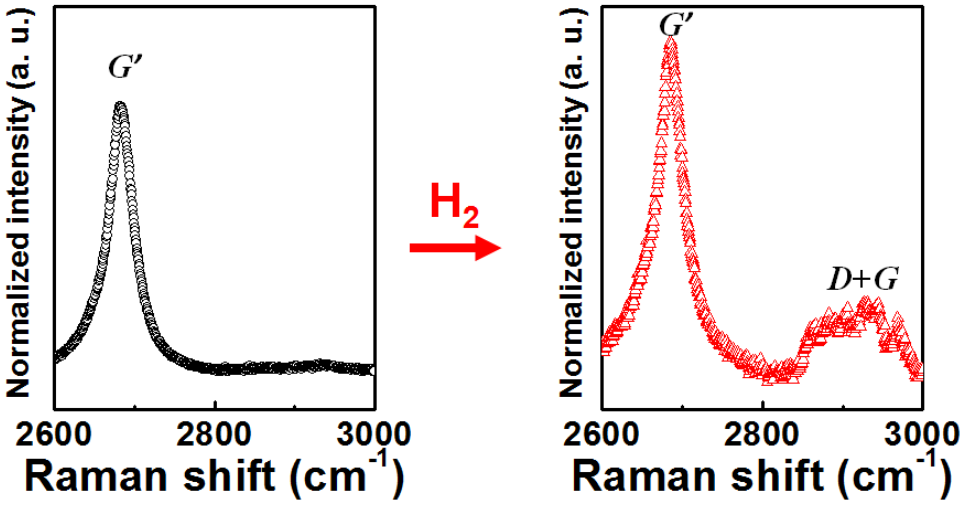

Figure 3.8 Raman spectra of the SWNTs before and after hydrogen exposure process. The spectra are normalized by the maximum value of the *G* mode at ~1592 cm^{-1} (data not shown).

We observed that the electron doping effect does not originate from physisorption of hydrogen molecule in the previous experiment in Fig. 3.3. To check the formation of C-H bond at the surface of SWNTs, Raman spectroscopy and XPS were performed. Figure 3.8 is the Raman spectra of the SWNTs before and after hydrogen exposure process. After H_2 exposure, *D* + *G* mode (at ~2930 cm^{-1})

develops, which is regarded as a fingerprint of hydrogenated graphitic layers [12, 35] . This indicates that the C-H bond acts as a medium to combine two different phonons (*D* and *G* mode) on SWNT [33, 34]. Comparing the *G* + *D* mode observed in our previous experiment with planar graphene [12, 35], the *G* + *D* mode in our SWNTs (Fig. 3.8) is reasonable because SWNTs have higher reactivity with hydrogen than graphene.

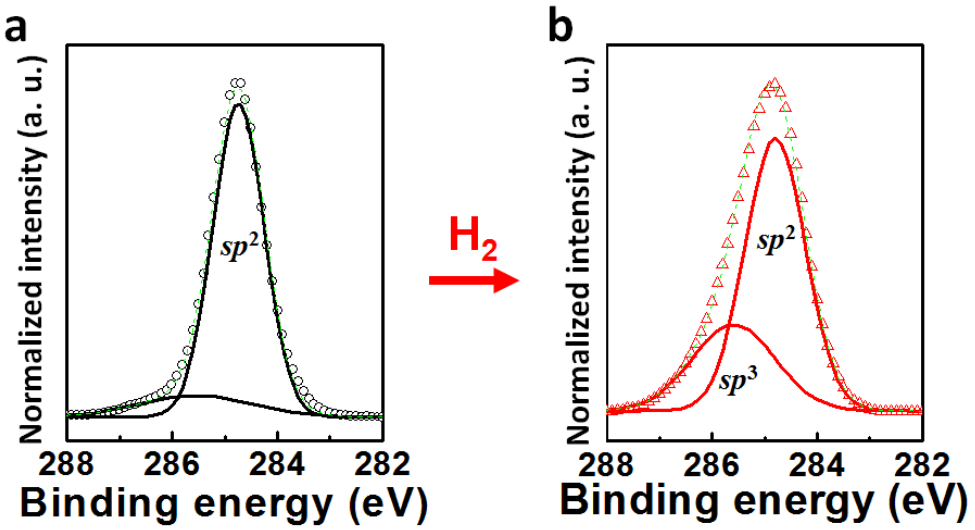

Figure 3.9 XPS C1s profiles of SWNTs. (a) before and (b) after hydrogen exposure process. The scatters are from raw data. The fitting curves according to the energy of sp^2 (at ~ 284.75 eV) and sp^3 (at ~285.55 eV) are presented as solid lines where the dashed green lines show the total envelops of the fitting line.

XPS is one of the mostly used techniques for characterization of C-H bond on the

graphitic surface. C1s XPS spectra normalized by the total area are shown in Fig. 3.9. The peak for sp^2 hybridization (at ~284.75 eV) is dominant before H_2 exposure as expected in usual graphitic materials (Fig. 3.9a), but the asymmetrically broadened C1s line was observed after H_2 exposure (Fig. 3.9b). This behavior is commonly shown in the hydrogenated graphitic materials employed by various methods, such as hydrogen atoms [36], hydrogen plasma [37, 38], and molecules [17]. The broadened peak means the formation of C-H bonds (sp^3 hybridization) after H_2 exposure.

Comparing the normalized (by the total C1s area) peak intensities, we can approximately estimate the composition of sp^2 and sp^3 hybridization of hydrogen-exposed SWNTs [39]. For the quantitative analysis, we decomposed the peak into to two subpeaks at ~285.55 eV and 284.75 eV [17] corresponding to the sp^3 and sp^2 hybridization, respectively [36]. The asymmetry of C1s peak in the pristine sample (before H_2 exposure) comes from the nature of graphitic materials which have π and σ bonds at the same time. Although, we just used the model of two picks (at 285.55 eV and 284.75 eV) because of the convenience of analysis. Indeed, we found that the model (green dashed line in Fig. 3.9a) is in acceptable regime.After the SWNT is exposed to high H_2 pressure, the peak at 285.55 eV corresponding to sp^3 hybridization significantly increases, which results from the formation of C-H bond on the surface of SWNT. The dramatically increases sp^3 hybridization after H_2 exposure is in accordance with the previous report on the hydrogenated SWNT [17, 36].

3.3.6 Electrical properties with covalent bond

In this section, we discuss the effect of covalent bond formation on the electronic properties of SWNT. It is expected that the conductivity becomes reduced when covalent bonds on the graphitic surface are formed. The transport of charge carrier on the graphitic surface heavily relies on the π orbital of carbon. Although the π orbital can be occupied by electron pair (two electrons), it is normally occupied by only one electron. So, it can be regarded as both one electron filled and one hole filled orbital. This system is well reflected in the special energy band structure, Dirac cone as discussed before. Occupation of hydrogen in one carbon site means the formation of covalent bond between π electron of carbon and σ electron of hydrogen [41]. So, formation of covalent bond consume a π orbital that contributes the transport of charge carriers.

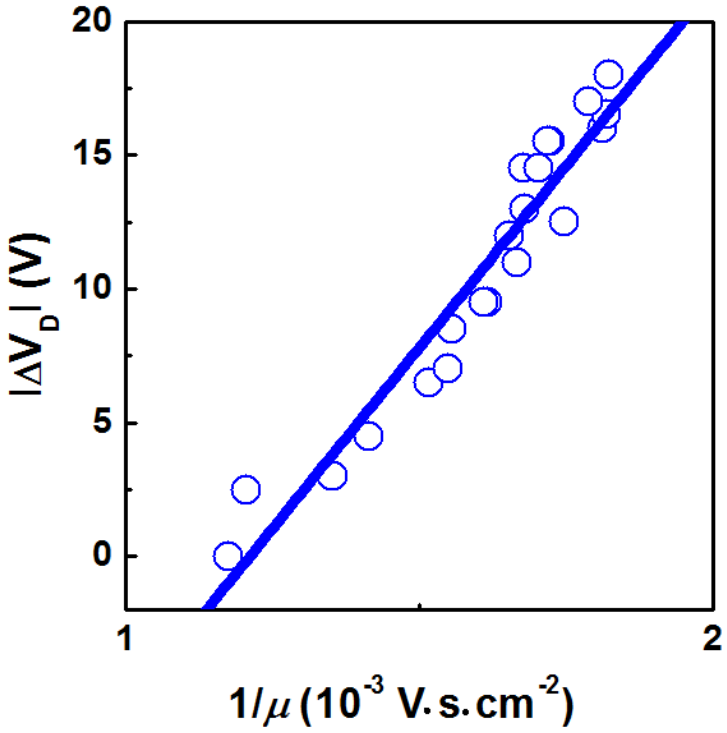

Figure 3.10 Short-range scattering of C-H bond on graphitic layer. The data is extracted from *in-situ* electrical measurements of H_2-exposed graphene device shown in Fig. 3.6d. The inverse field-effect mobility ($1/\mu$, x-axis) was obtained from the slope of I_{ds}-V_{gs} curve at the $V_{gs} = V_D$ - 15 V (blue circles). The linear dependance (blue line) represents the theoretical expectaion of short-range scattering phenomenon in graphene devices [42].

Figure 3.10 is the V_D shift with respect to the inverse field-effect mobility of hole-type charge carriers. We observed asymmetrical field-effect mobility change as observed in single-layer graphene devices [5, 8]. The asymmetrical mobility

change is believed to be originated from the reaction of substrate and hydrogen gas [43]. Hence, we used the hole-type charge carriers for the analysis. It is note worthy that the shifted curve is proportional to the impurity density of graphene (n_{imp}) with relationship of $n_{imp} = \frac{\delta \cdot c_g}{e}\left|\Delta V_D\right|$, where δ is amount of doped charge per C-H bond and e is the unit charge, and c_{g} is unit capacitance between graphene and Si gate. According to the theoretical report, the impurity density of short-range scatterer is inversely proportional to the mobility [42]. It is well accepted that the C-H bond act as as short-range scattering site on the graphitic surface [5]. Although the long-range scattering is also presented by the same relationship, the result depicted in Fig. 3.10 originates from short-range scaterrer because we already verified the formation of C-H bond *via* XPS and Raman spectroscopy as discussed before (Fig. 3.8, Fig. 3.9). Therefore, the linear relation of ΔV_{D} vs $1/\mu$ in Fig. 3.10 fulfills the necessary condition of the short-range scattering site as expected from the C-H covalent bond formation on the surface [5].

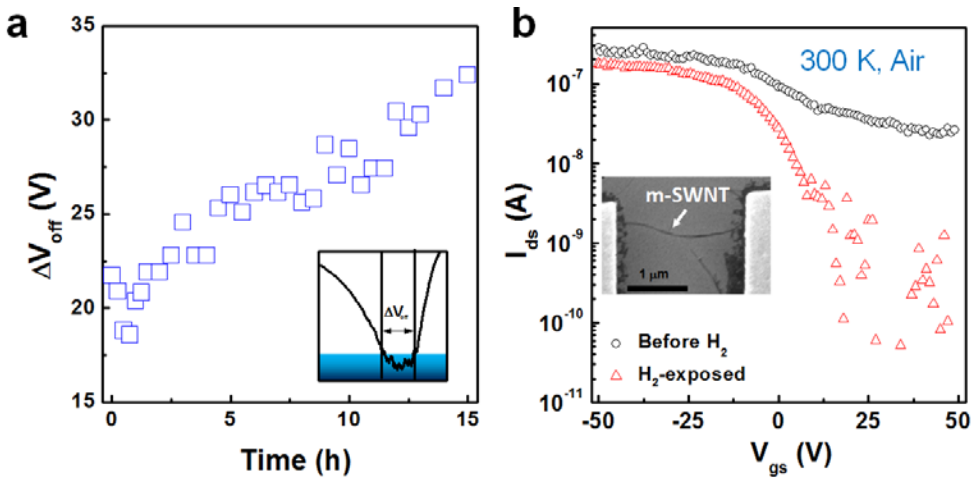

Figure 3.11 Electronic property change of hydrogen-exposed SWNT due to the formation of C-H covalent bond. (a) Off-state widening of semiconducting SWNT with respect to the hydrogen exposure time. The data is extracted from the *in-situ* electrical measurements shown in Fig. 3.5. ΔV_{off} is defined by the difference of gate voltage having the current of ~200 pA in the I_{ds}-V_{gs} curve as described in the inset. (b) The I_{ds}-V_{gs} curve of metallic SWNT before (black circles) and after (red triangles) hydrogen exposure process. Both measurements were performed under ambient air condition. Inset shows the top view of the device obtained by SEM imaging. V_{ds} is fixed to 0.1 V

In the previous experiement on the semiconducting SWNT FET, we observed broadening of the minimum conduction regime. In Fig. 3.5, blue colored minimum conduction regime of the device was broadened as incresing hydrogen exposure time. So, we defined the difference of gate voltage having the current of ~200 pA in the I_{ds}-V_{gs} curve as off-state width (ΔV_{off}) as shown in inset of Fig. 3.11a. The ΔV_{off} with respecto to the hydrogen exposure time is shown in Fig. 3.11a.

It was experimentally reported that hydrogenated metallic SWNTs show the evidence of energy band gap widening, the increased on-off ratio in the electrical measurements [14, 28]. For the comprehansive understanding on this effect, we perform the hydrogen gas exposure experiment on the metallic SWNT. Inset of Fig. 3.11b shows the SEM image of metallic SWNT on hBN device fabricated using the same techniques (with the semiconducting SWNT FET). Although we used 99% semiconducting SWNT solution containing only 1% of metallic SWNT, we often obtain metallic SWNT device due to the much higher electrical permitivity of metallic SWNT ($\varepsilon_r \sim \infty$) than semiconducting SWNT ($\varepsilon_r \sim 5$) [44].

Figure 3.11b is the I_{ds}-V_{gs} curve of metallic SWNT before (black circles) and after (red triangles) hydrogen exposure process. Both measurements were performed under ambient air condition. The pristine SWNT device shows very small gate voltage dependence of drain-source current. It is a typical electrical signal expected from metallic SWNT [14, 28]. Due to the DOS of the metallic SWNT is continuous without gap, the current can flow wherever the Fermi level is located. However, after the high-temperature (400 K), high-pressure (20 bar) hydrogen exposure process, the SWNT FET shows significant gate voltage dependence of I_{ds} as presented by red triangles in Fig. 3.11b.

Our observation on Fig. 3.11b is attributed to the electronic bandstructure changed by C-H bond formation on SWNT surface. The theoretical background of energy band gap widening from previous report [28] is shown in Fig. 3.12a. Kim *et al.* have reported that DFT calculation on amchair SWNT with C-H bond shows changed energy band structure with energy band gap widening [28]. They showed

that the sp^3 hydridization caused by hydrogenation of graphitic layer removes the π bands near the Fermi level of SWNT, and it leads the widened energy band gap [28]. Zhang *et al.* experimentally verified the band gap opening of the metallic SWNT device *via* hydrogenation [14]. Hydrogenated metallic SWNT showed increased on-off ratio according to the widened energy band gap. The observed off-state widening is in consistant with our observations such as increased on-off ratio hydrogen gas-exposed metallic SWNT, increased *D*+*G* mode in Raman spectroscopy (Fig. 3.8), and increased sp^3 peak on XPS (Fig. 3.9).

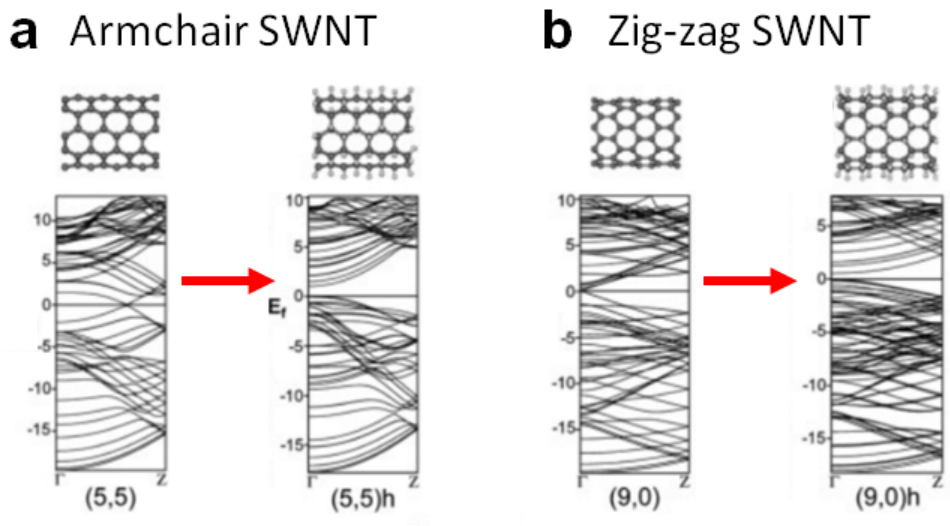

Figure 3.12 Theoretical calculation on energy band structure of (a) armchair and (b) zig-zag SWNT before and after hydrogenation. The upper images show the structural model of SWNT. Adapted from Ref.[28].

Not only metallic armchair SWNT, but also zig-zag SWNT is expected to shows

the band gap widening due to the π bands removing effect (Fig. 3.12b) [28]. Therefore, our observation of off-state widening on semiconducting SWNT FET after hydrogen exposure process (Fig. 3.11a) can be explained in this manner. As mentioned in introduction section, application of SWNT is mostly focused on the semiconducting SWNT. Although the metallic SWNT have alternatives such as graphene, semiconducting SWNT is one of the most promising materials for the next generation electronics. So, this kind of band gap opening, and widening can be useful for the future applications.

3.3.7 SWNT network FET exposed to hydrogen

To check the electron doping effect on the SWNT network FET that is more appropriate for the scalable fabrication, we performed the hydrogen exposure process on the SWNT network FET as shown in Fig. 3.13. Since the random networks are made by the drop-casting method using 99% semiconducting SWNTs, the semiconducting network device can easily be obtained. Combining with the conventional fabrication technique for the scalable gold electrode arrays, this type of device has a possiblity of scalability.

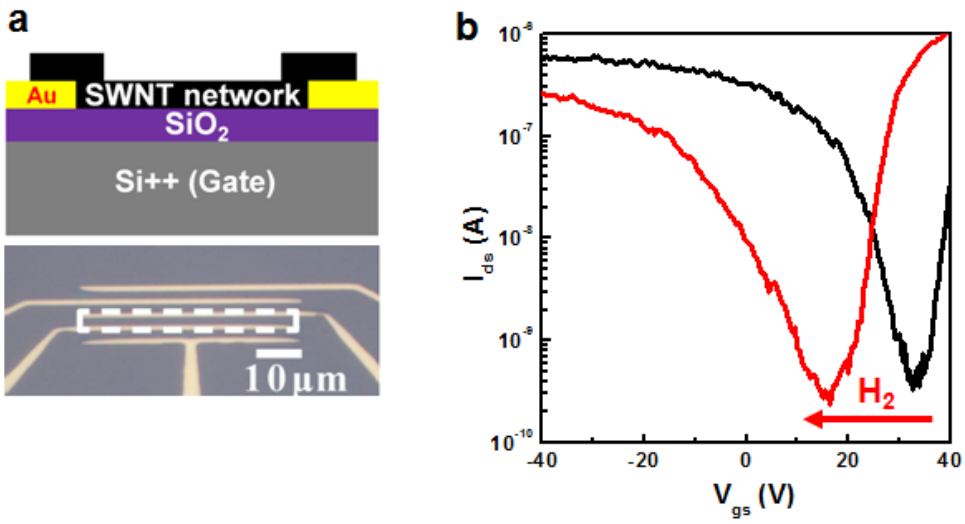

Figure 3.13 Application to the SWNT network FET. (a) Schematic image of cross-sectional view of SWNT device. The top view of optical image is below. Dashed white line presents the network channel area between electrodes. Semiconducting SWNT was deposited onto the pre-patterned gold electrodes on SiO_2 substrate by drop-casting method [45]. (b) I_{ds}-V_{gs} curve before and after high-pressure (20 bar) hydrogen exposure at 400 K for 15 h .

Figure 3.13b shows the *in-situ* I_{ds}-V_{gs} curve measurements before and after hydrogen exposure. As hydrogen was exposed to network device, the I_{ds}-V_{gs} curve shifts to the negative gate side suggesting more electron doped on the SWNT surface. The result is in accordance with the elctron doping effect of the SWNT network observed by KPFM in Fig. 3.4. Because this type of device can be scaled up, we expect the electron doping effect can be applied to the scalable SWNT FET arrays that are suitable for the applications.

3.4 Summary of Chapter 3

In summary, we demonstrated high-pressure and high-temperature hydrogen exposure process to the semiconducting SWNTs. The extrinsic effects caused by environmental conditions were ruled out by using two-dimensional hBN substrate and *in-situ* measurements. The electron doping effect was observed by the shifted I_{ds}-V_{gs} curve of SWNT FET and Kelvin probe force microscopy (KPFM). The changed electronic properties were maintained at room temperature under vacuum condition at least for 24 h showing it does not originate from physisorption. Comparing to the planar graphene sheet device, we observed the curved structure of SWNT is advantages on hydrogenation as predicted by theoretical study [13, 14]. XPS and Raman spectroscopy verified the formation of C-H bond on SWNT surface after the hydrogen exposure process. The covalent bond yields short-range scattering in the graphene device and band gap widening in the SWNT devices. Finally, a demonstration of the hydrogen gas-exposure technique for the random network SWNT FET opens the possibility of scalable fabrication of electron doping on the SWNT hydrogen exposure process.

Bibliography

[1] Vergés J and de Andres P 2010 Trapping of electrons near chemisorbed hydrogen on graphene *Physical Review B* **81** 075423

[2] Matis B R, Burgess J S, Bulat F A, Friedman A L, Houston B H and Baldwin J W 2012 Surface doping and band gap tunability in hydrogenated graphene *ACS nano* **6** 17-22

[3] Zhu Z H, Lu G Q and Wang F Y 2005 Why H atom prefers the on-top site and alkali metals favor the middle hollow site on the basal plane of graphite *The Journal of Physical Chemistry B* **109** 7923-7

[4] Rossi A, Piccinin S, Pellegrini V, de Gironcoli S and Tozzini V 2015 Nano-scale corrugations in graphene: a density functional theory study of structure, electronic properties and hydrogenation *The Journal of Physical Chemistry C* **119** 7900-10

[5] Katoch J, Chen J-H, Tsuchikawa R, Smith C W, Mucciolo E R and Ishigami M 2010 Uncovering the dominant scatterer in graphene sheets on SiO 2 *Physical Review B* **82** 081417

[6] Ryu S, Han M Y, Maultzsch J, Heinz T F, Kim P, Steigerwald M L and Brus L E 2008 Reversible basal plane hydrogenation of graphene *Nano letters* **8** 4597-602

[7] Sato Y, Takai K and Enoki T 2011 Electrically controlled adsorption of oxygen in bilayer graphene devices *Nano letters* **11** 3468-75

[8] Kim B H, Hong S J, Baek S J, Jeong H Y, Park N, Lee M, Lee S W, Park M, Chu S W and Shin H S 2012 N-type graphene induced by dissociative H 2 adsorption at room temperature *Scientific reports* **2** 1-6

[9] Hong S J, Park M, Kang H, Lee M, Soler-Delgado D, Jeong D H, Park Y W and Kim B H 2016 Manipulation of electrical properties in CVD-grown twisted bilayer graphene induced by dissociative hydrogen adsorption *Current Applied Physics* **16** 1637-41

[10] Hong S J, Park M, Kang H, Lee M, Soler-Delgado D, Shin D S, Kim K H, Kubatkin S, Jeong D H and Park Y W 2015 Verification of electron doping in single-layer graphene due to H2 exposure with thermoelectric power *Applied Physics Letters* **106** 142110

[11] Hong S, Kim H, Lee M, Kang H, Park M, Jeong D, Lee S, Park Y and Kim B 2017 Chemical manipulation of edge-contact and encapsulated graphene by dissociated hydrogen adsorption *RSC advances* **7** 6013-7

[12] Hong S, Kang H, Park M, Lee M, Soler-Delgado D, Jeong D, Park Y and Kim B 2015 Competition between electron doping and short-range scattering in hydrogenated bilayer graphene on hexagonal boron nitride *RSC advances* **5** 103276-9

[13] Park S, Srivastava D and Cho K 2003 Generalized chemical reactivity of curved surfaces: carbon nanotubes *Nano letters* **3**

1273-7
[14] Zhang G, Qi P, Wang X, Lu Y, Mann D, Li X and Dai H 2006 Hydrogenation and hydrocarbonation and etching of single-walled carbon nanotubes *Journal of the American Chemical Society* **128** 6026-7
[15] Chen Y-F and Fuhrer M S 2006 Tuning from thermionic emission to ohmic tunnel contacts via doping in Schottky-barrier nanotube transistors *Nano letters* **6** 2158-62
[16] Derycke V, Martel R, Appenzeller J and Avouris P 2002 Controlling doping and carrier injection in carbon nanotube transistors *Applied Physics Letters* **80** 2773-5
[17] Talyzin A V, Luzan S, Anoshkin I V, Nasibulin A G, Jiang H, Kauppinen E I, Mikoushkin V M, Shnitov V V, Marchenko D E and Noreus D 2011 Hydrogenation, purification, and unzipping of carbon nanotubes by reaction with molecular hydrogen: road to graphane nanoribbons *Acs Nano* **5** 5132-40
[18] Do Thanh L and Balk P 1988 Elimination and Generation of Si-SiO2 Interface Traps by Low Temperature Hydrogen Annealing *Journal of The Electrochemical Society* **135** 1797-801
[19] Xue W and Li P 2011 Dielectrophoretic deposition and alignment of carbon nanotubes *Carbon Nanotubes—Synthesis, Characterization, Applications; Yellampalli S., editor., Ed* 171-90
[20] Krupke R, Hennrich F, Löhneysen H v and Kappes M M 2003 Separation of metallic from semiconducting single-walled carbon nanotubes *Science* **301** 344-7
[21] Sarker B K, Shekhar S and Khondaker S I 2011 Semiconducting enriched carbon nanotube aligned arrays of tunable density and their electrical transport properties *ACS nano* **5** 6297-305
[22] Heller I, Janssens A M, Männik J, Minot E D, Lemay S G and Dekker C 2008 Identifying the mechanism of biosensing with carbon nanotube transistors *Nano letters* **8** 591-5
[23] Radosavljević M, Appenzeller J, Avouris P and Knoch J 2004 High performance of potassium n-doped carbon nanotube field-effect transistors *Applied Physics Letters* **84** 3693-5
[24] Henwood D and Carey J D 2007 Ab initio investigation of molecular hydrogen physisorption on graphene and carbon nanotubes *Physical Review B* **75** 245413
[25] Fuller E J, Pan D, Corso B L, Gul O T and Collins P G 2014 Mean free paths in single-walled carbon nanotubes measured by Kelvin probe force microscopy *Physical Review B* **89** 245450
[26] Pankove J, Lampert M and Tarng M 1978 Hydrogenation and dehydrogenation of amorphous and crystalline silicon *Applied Physics Letters* **32** 439-41
[27] Kang H, Hong S J, Park M, Jang H-S, Nam K, Choi S, Kim B H and Park Y W 2018 Tuning the electronic structure of single-walled

carbon nanotube by high-pressure H2 exposure *Nanotechnology* **30** 065201

[28] Kim K S, Bae D J, Kim J R, Park K A, Lim S C, Kim J J, Choi W B, Park C Y and Lee Y H 2002 Modification of electronic structures of a carbon nanotube by hydrogen functionalization *Advanced Materials* **14** 1818-21

[29] Ilani S and McEuen P L 2010 Electron transport in carbon nanotubes *Annu. Rev. Condens. Matter Phys.* **1** 1-25

[30] Calvi A, Ferrari A, Sbuelz L, Goldoni A and Modesti S 2016 Recognizing physisorption and chemisorption in carbon nanotubes gas sensors by double exponential fitting of the response *Sensors* **16** 731

[31] Ciammaruchi L, Bellucci L, Castillo G C, Sánchez G M-D, Liu Q, Tozzini V and Martorell J 2019 Water splitting for hydrogen chemisorption in graphene oxide dynamically evolving to a graphane character lattice *Carbon* **153** 234-41

[32] Russo C J and Passmore L A 2014 Controlling protein adsorption on graphene for cryo-EM using low-energy hydrogen plasmas *Nature Methods* **11** 649-52

[33] Meletov K, Bashkin I, Shestakov V, Krestinin A, Davydov V, Pulikkathara M, Khabashesku V, Arvanitidis J, Christofilos D and Kourouklis G 2008 Raman study of hydrogenated and fluorinated single-walled carbon nanotubes *Fullerenes, Nanotubes and Carbon Nanostructures* **16** 322-9

[34] Meletov K, Maksimov A, Tartakovskii I, Bashkin I, Shestakov V, Krestinin A, Shulga Y M, Andrikopoulos K, Arvanitidis J and Christofilos D 2007 Raman study of the high-pressure hydrogenated single-wall carbon nanotubes: In search of chemically bonded and adsorbed molecular hydrogen *Chemical physics letters* **433** 335-9

[35] Kim B H, Hong S J, Baek S J, Jeong H Y, Park N, Lee M, Lee S W, Park M, Chu S W and Shin H S 2012 N-type graphene induced by dissociative H 2 adsorption at room temperature *Scientific reports* **2** 690

[36] Nikitin A, Ogasawara H, Mann D, Denecke R, Zhang Z, Dai H, Cho K and Nilsson A 2005 Hydrogenation of single-walled carbon nanotubes *Physical review letters* **95** 225507

[37] Lee E-s, Lim Y-K, Chun Y-s, Wang B-Y and Lim D-S 2017 Characteristics of hydrogen plasma treated carbon nanotubes and their influence on the mechanical properties of polyetherimide-based nanocomposites *Carbon* **118** 650-8

[38] Jayasingha R, Sherehiy A, Wu S-Y and Sumanasekera G 2013 In situ study of hydrogenation of graphene and new phases of localization between metal–insulator transitions *Nano letters* **13** 5098-105

[39] Nilsson A 2002 Applications of core level spectroscopy to adsorbates *Journal of electron spectroscopy and related phenomena*

126 3-42
[40] Okpalugo T, Papakonstantinou P, Murphy H, McLaughlin J and Brown N 2005 High resolution XPS characterization of chemical functionalised MWCNTs and SWCNTs *Carbon* **43** 153-61
[41] Han S S and Lee H M 2004 Adsorption properties of hydrogen on (10, 0) single-walled carbon nanotube through density functional theory *Carbon* **42** 2169-77
[42] Ferreira A, Viana-Gomes J, Nilsson J, Mucciolo E R, Peres N M and Neto A C 2011 Unified description of the dc conductivity of monolayer and bilayer graphene at finite densities based on resonant scatterers *Physical Review B* **83** 165402
[43] Silvestre I, de Morais E A, Melo A O, Campos L C, Goncalves A-M B, Cadore A R, Ferlauto A S, Chacham H, Mazzoni M S and Lacerda R G 2013 Asymmetric effect of oxygen adsorption on electron and hole mobilities in bilayer graphene: long-and short-range scattering mechanisms *ACS nano* **7** 6597-604
[44] Krupke R, Hennrich F, Kappes M M and v. Löhneysen H 2004 Surface conductance induced dielectrophoresis of semiconducting single-walled carbon nanotubes *Nano letters* **4** 1395-9
[45] Kybert N J, Lerner M B, Yodh J S, Preti G and Johnson A C 2013 Differentiation of complex vapor mixtures using versatile DNA-carbon nanotube chemical sensor arrays *ACS nano* **7** 2800-7

Chapter 4

Hydrogen-exposed SWNT FETs with low work function metal contacts

4.1 Introduction

4.1.1 Schottky barrier formation of SWNT with low work function metal contacts

The height of Schottky barrier (SB) is defined as ${}^{n}\Phi_{SB} = \Phi_{M} - \chi$ for electron injection and ${}^{p}\Phi_{SB} = I - \Phi_{M}$ for hole injection. χ is electron affinity of SWNT that is the energy needed to remove an electron from the conduction band minimum and I is ionization energy that represents the energy difference of valence band maximum and vacuum level. It is noteworthy that the sum of SB heights for electron and hole injection is equal to the energy band gap of semiconductor. ${}^{n}\Phi_{SB} + {}^{p}\Phi_{SB} = (\Phi_{M} - \chi) + (I - \Phi_{M}) = E_{g}$. However, in case of real devices, there are interface states such as defects on the semiconductor surface, charge traps, and lattice miss match with metal contacts. These interface state make the influence of metal work function on height of SB less effective.

Although the overall tendency follows the barrier height expected from the Schottky–Mott rule, we always have to consider the effect from interface state. Figure 4.1 shows the previous experimental results on the SB height dependence on work function of contact metal (adapted from Ref.[1]). The dashed line represents the total dependence (equal to the slope 1 of previous discussion in Chapter 1) of SB height. Due to the presence of interface states between SWNT and metal contact the slope is not 1, but some value between 1 and 0 is expected. Only SWNT with large diameter (2.5 nm, black squares) shows the slope near to 0 due to the small energy band gap. The manufacturer of SWNT (IsoNanotubes-S, Nanointegris inc.) guarantees the range of SWNT diameter between 1.2 nm ~ 1.7 nm and we observed 1.2 nm of the diameter using AFM (Fig.4.7b). Therefore, the 1 nm ~ 2 nm cases in Fig. 4.3 can be comparable to our devices.

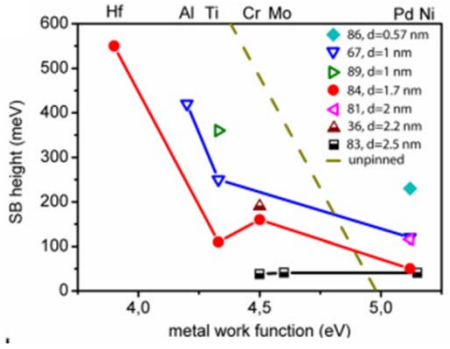

Figure 4.1 References showing that SB height depending on contact metal work function according to its diameter. Adapted from Ref.[1].

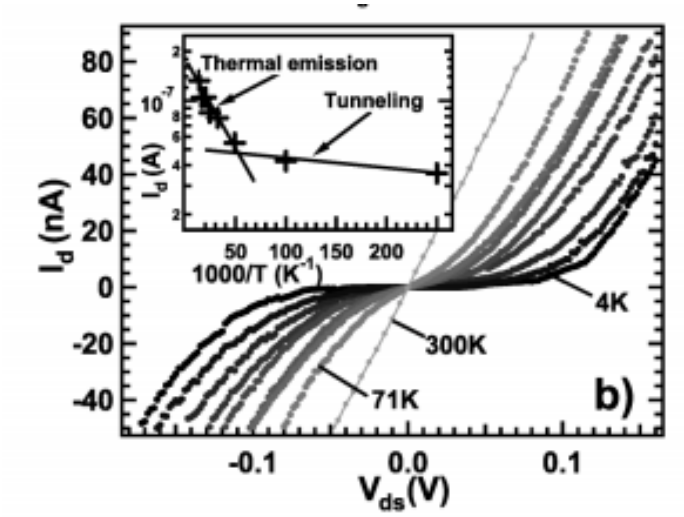

Figure 4.2 SB thinning in SWNT FET devices with applied gate voltage. Adapted from Ref.[2].

Figure 4.2 shows SB thinning in SWNT FET devices with applied gate voltage. Because Au have higher work function than SWNT, hole favorable SB (${}^{n}\Phi_{SB} > {}^{p}\Phi_{SB}$) are expected at the Au contacted SWNTs. However, in case of low Φ_M metal contact, the heights of SB can be inverted forming electron favorable SB (${}^{n}\Phi_{SB} < {}^{p}\Phi_{SB}$) where the summation of height of SB remains constant (E_g). Figure 4.3 shows the schematic energy band diagram of SWNT with low Φ_M metal contact. The height of ${}^{p}\Phi_{SB}$ is expected to be larger in this scheme. However, the barrier can become very thin when negative gate voltage is applied. Because the ${}^{p}\Phi_{SB}$ can be thinned until it is nearly transparent to the thermionic-field emission of charge carriers [3, 4], the ambipolar nature of SWNT is observed in this low Φ_M metal

contacted system regardless of contact metals. [5].

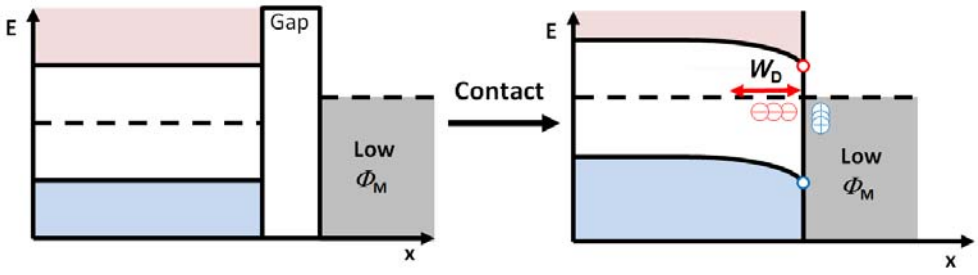

Figure 4.3 Schematic energy band diagram of SWNT with low Φ_M metal contact.

4.1.2 Strategies for *n*-type SWNT FETs: Electron doping and contact engineering

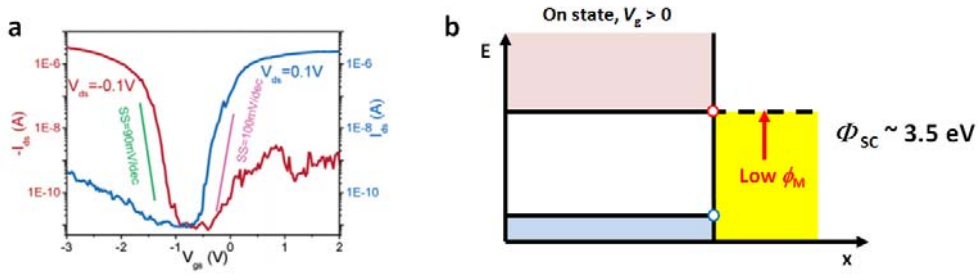

Figure 4.4 SB *n*-type SWNT FET using Sc electrodes. (a) Comparison of I_{ds}-V_{gs} curves of SWNT with Pd electrodes (red, left axis) and Sc electrodes (blue, right axis) adapted from Ref.[6]. (b) Expected energy band diagram of the SB *n*-type FET at the on state with positive gate voltage.

In case of the "significantly" low Φ_M contact metal such as Sc (Φ_M ~ 3.5 eV), ${}^n\Phi_{SB}$ become very small and ${}^p\Phi_{SB}$ become very large. Due to the high ${}^p\Phi_{SB}$, both tunneling and thermionic emission of hole-type charge carrier are affected. Since SB thinning by applying gate voltage is not enough to allow transport of the hole type charge carrier (due to the significantly high ${}^p\Phi_{SB}$), this type of device can show perfect *n*-type FET. Zhang *et al.* have reported *n*-type SWNT device with Sc contact. The key insight of the method is manipulation of SB resulting in electron favorable contact to the SWNTs, which makes ${}^n\Phi_{SB}$ nearly zero. Therefore, only electron injection from the contact metal is possible, while hole injection is prohibited. It shows ohmic contact to the electron injection and Schottky contact to the hole injection in the wide range of temperatures. This strategy is clearly distinguished from the more intuitive method for achieving *n*-type FET, electron doping.

Alkali metals are classical and efficient materials for the electron doping. Due to the considerably low electronegativity, the alkali metals tend to donate the electrons to the other materials. M. Radosavljevic *et al.* have reported that electron doping effect on K vapor treated SWNT FET (Fig. 4.5a). Figure 4.5a shows the I_{ds}-V_{gs} curve with stepwise K vapor exposure process. The numbers marked in curves represent the cycles of K vapor treatment. As the number of vapor exposure cycle increases, the I_{ds}-V_{gs} curve shifts to the negative gate voltage side as in case of our hydrogen exposure on SWNT in Fig. 3.2c.

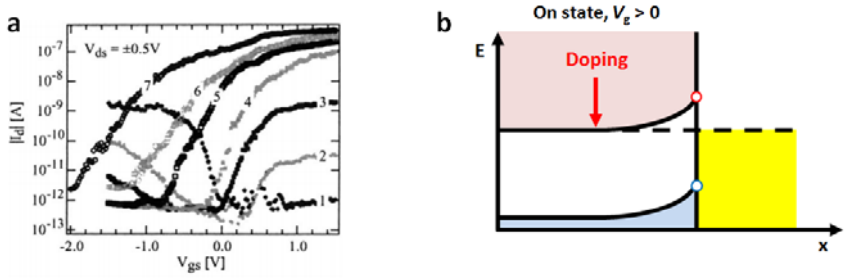

Figure 4.5 *n*-type SWNT FET with electron doping method. (a) I_{ds}-V_{gs} curves of K vapor-exposed SWNT FET. The numbers represent the cycle of K vapor treatments. Adapted from Ref.[7]. (b) Expected energy band diagram of the electron-doped SWNT FET at the on state with positive gate voltage.

4.2 Experimental

To reduce the extrinsic effect from oxide substrates [8], few layer hBN was used for the substrate of SWNT FETs. After exfoliation of hBN by scotch tape method, SWNTs were deposited onto the hBN using drop-casting method [9]. After rinsing with DI water and IPA, the SWNTs were identified by SEM imaging. Figure 4.6a is the SEM image of SWNT deposited onto the hBN on SiO_2 substrate. The hBN substrates are preferred for the adsorption of SWNTs than normal SiO_2 substrates. After locating the single strand SWNTs on the hBN, we performed e-beam lithography as described before in the Chapter 3. We deposited 3 nm ~5 nm Cr and 20 nm Au for the Cr-contacted SWNT FET. ~10 nm Ti and 20 nm Au were

deposited for the Ti-contacted SWNT FET. Figure 4.6b is a SEM image of the final device. Single strand SWNT on hBN was electrically connected to the metal contacts.

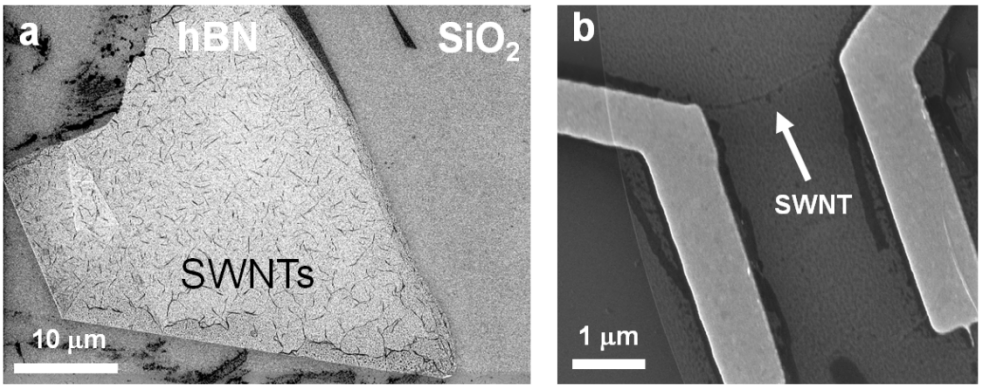

Figure 4.6 FE-SEM image of (a) SWNTs deposited onto the exfoliated hBN, and (b) final FET device.

The device was mounted to the high-pressure, high-temperature chamber for *in-situ* electrical measurements. After at least 10 h of degassing process at 400 K under ~$2 \cdot 10^{-6}$ torr dynamic vacuum condition, the device was exposed to the high-pressure hydrogen gas (20 bar). The whole process was monitored by 3-terminal electrical measurements using Keithley 4200 semiconductor characterization system. For the Cr-contacted device, drain-source current at the fixed drain-source voltage (0.1 V) depending on gate-source voltage sweep from +50 V to -50 V was measured every 30 min for total 23 h of hydrogen exposure process. For the Ti-

contacted device, drain-source current at the fixed drain-source voltage (0.1 V) depending on gate-source voltage round sweep from +50 V to -50 V was measured under the vacuum condition (~$2 \cdot 10^{-6}$ torr) before and after 24 h of hydrogen exposure.

4.3 Results and discussion

4.3.1 Hydrogen exposure of SWNT FETs with different metal contacts

In the previous chapter, we observed the electron doping effect on SWNT exposed to hydrogen gas. Although the electron doping effect is useful in terms of tuning the Fermi level, the resulted device still showed ambipolar transport that is not appropriate for utilizing as an *n*-type FET. In this section, we propose contact engineering technique combining with hydrogen exposure that effectively reduce the hole injection resulting in appropriately working *n*-type FET.

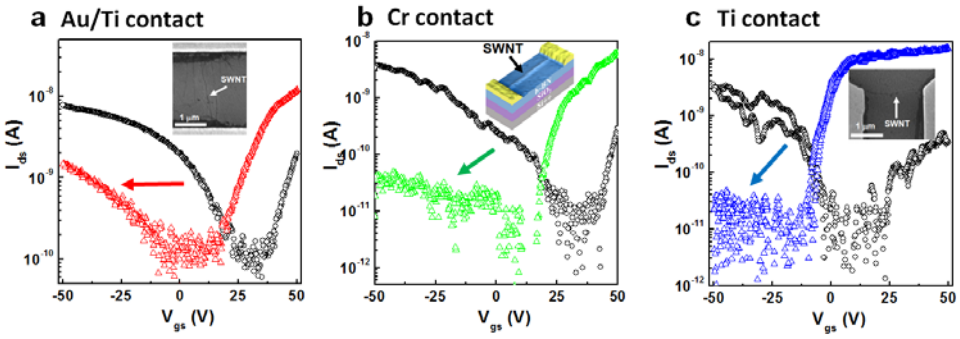

Figure 4.7 Hydrogen exposure experiments of SWNT FETs with different metal contacts. (a) I_{ds}-V_{gs} curve of Au/Ti-contacted SWNT FET before (black circles) and after (red triangles) hydrogen exposure. Inset is the SEM image of the device. (b) Cr-contacted SWNT FET before (black circles) and after (green triangles) hydrogen exposure. Inset is the 3D AFM image of the device. (c) Ti-contacted SWNT FET before (black circles) and after (blue triangles) hydrogen exposure. Inset is the SEM image of the device.

Figure 4.7 shows the I_{ds}-V_{gs} characteristics of SWNT FETs with different metal contacts after exposure to high pressure H_2. I_{ds}-V_{gs} curves of SWNT FETs degassed at 400 K for 10 h are presented as black circles (Fig. 4.7). All devices shows ambipolar behavior regardless of the contact metals as previously reported [2, 5]. It is well known that Schottky barrier (SB) of SWNT device can be nearly transparent with the applied gate voltage [2]. So, usually, the I_{ds}-V_{gs} curves of SWNT FET does not reflect the difference of contact metal work function as different heights of SB can be ignored when they are too thin [2].

On the other hand, the hydrogen-exposed devices show the different responses according to the different contact methods. We observed the reduction of hole-type carrier injection with the Cr and Ti contacts, after the SWNT FETS are exposed to high-pressure H_2 gas (20 bar) at high-temperature (400 K) for 15 h. The Au/Ti-contacted SWNT FET shows shifted I_{ds}-V_{gs} curve with small slope change (red triangles of Fig. 4.7a). However, Cr-contacted SWNT FET exposed to hydrogen gas shows shifted I_{ds}-V_{gs} curves with slope change at the left side of the curve corresponding to the hole injection (green triangles of Fig. 4.7b). In case of Ti-contact, the hydrogen exposure causes more significant slope change of I_{ds}-V_{gs} curve corresponding to the hole injection (blue triangles of Fig. 4.7c) leading to final *n*-type SWNT FET. More details on the difference of SB changes with different contact metals are discussed in the following section.

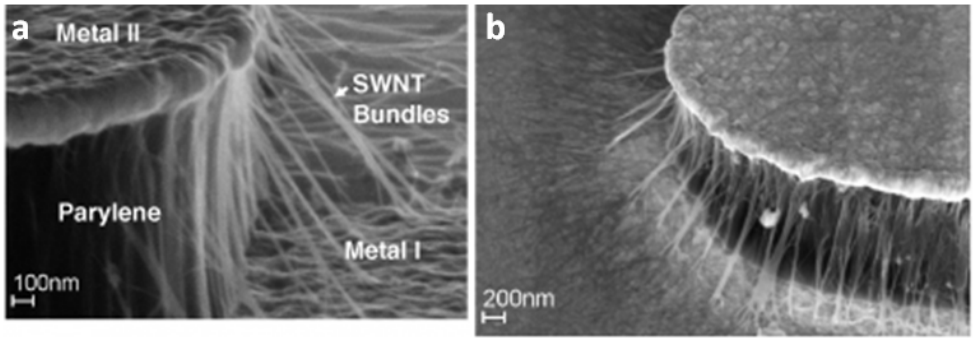

Figure 4.8 SEM image of DEP generated SWNT device adapted from Ref.[10].

It is noteworthy that the Cr- and Ti-contacted devices were made of top contact

method (SWNT deposition followed by metallization) while the Au/Ti contact was made of DEP technique (Fabrication of metal electrode followed by SWNT deposition using DEP). The DEP results in SWNT mainly contacted to top surface of metal electrodes (Fig. 4.8). So, in case of At/Ti-contacted SWNT FET, the most of SWNT are supposed to contact to Au surface, and no or small area of SWNT can contact to Ti side wall as depicted in Fig. 4.9a. The circuit diagram of the FET is shown in Fig. 4.9b [11]. R_{SWNT} is resistance of SWNT channel, and ΔR_{SWNT} is resistance of ~5 nm length of SWNT (Ti-contacted region of SWNT). $R_{C\text{-}Au}$ is contact resistance between Au and SWNT, and $R_{C\text{-}Ti}$ is contact resistance between Ti and SWNT. So, the total contact resistance can be regarded as parallel connection of $R_{C\text{-}Au}$ + ΔR_{SWNT} and $R_{C\text{-}Ti}$ (Fig. 4.9b) [11]. If one of the resistors becomes very large, the other can predominantly contribute the charge injection.

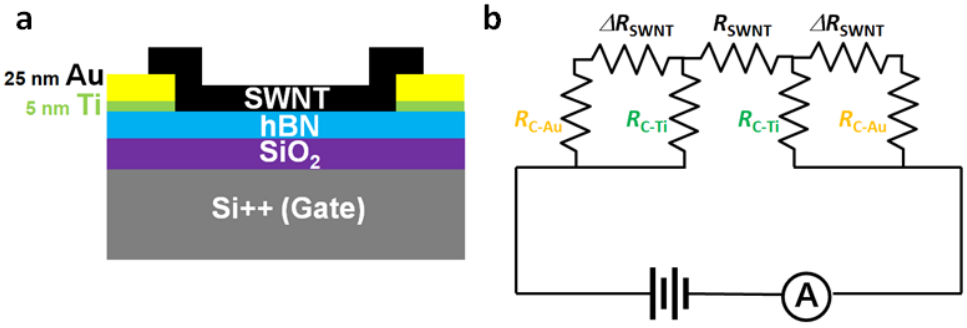

Figure 4.9 Diagrams of Au/Ti-contacted SWNT FET. (a) Schematic diagram of cross-sectional view of the DEP generated SWNT device with Au (~25 nm)/Ti (~5 nm) contact. (b) Circuit diagram of the device. R_{SWNT} is resistance of SWNT channel, and ΔR_{SWNT} is resistance of Ti contacted region of SWNT (~5 nm length

of SWNT). $R_{C\text{-}Au}$ is contact resistance between Au and SWNT, and $R_{C\text{-}Ti}$ is contact resistance between Ti and SWNT.

4.3.2 Electron doping induced significant reduction of the hole injection in Cr-contacted SWNT FET

According to Schottky-Mott rule, the height of SB is defined as ${}^{n}\Phi_{SB} = \Phi_M - \chi$ for electron injection, and ${}^{p}\Phi_{SB} = I - \Phi_M$ for hole injection. Although the height of SB is not supposed to be changed in the ideal case, the thickness of SB can significantly be changed with respect to the doping level [1]. Leonard *et al.* have reported that the depletion width of SWNT varies exponentially with inverse doping density with the relationship $W_D \propto \exp(A \cdot E_g/D)$ where D is the doping density and A is a constant [12]. The depletion width decides the thickness of SB.

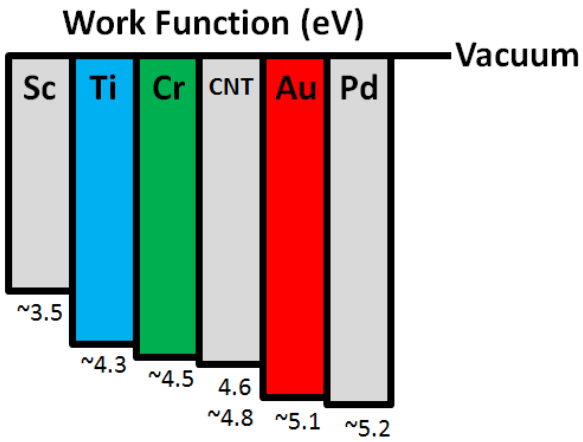

Figure 4.10 Comparison of work function of the metals that used for SWNT electrical contact. Values are adapted from Ref.[13].

Figure 4.10 is diagram of work function of metals that are used for SWNT contacts. Among the various types of contact metals, the work function of Cr with clean surface is known to be very similar with that of SWNT. Taking the interface state effect (Fig. 4.1) account, nearly same height of SBs are expected for hole and electron injection [14].

Figure 4.11 shows the doping dependent SB change on Cr-contacted SWNT FET reported by Chen *et al.* They verified that only small amount of hole doping can drastically change the 'neutral' device to nearly perfect *p*-type semiconductor device due to the considerable thickness change of SBs [14].

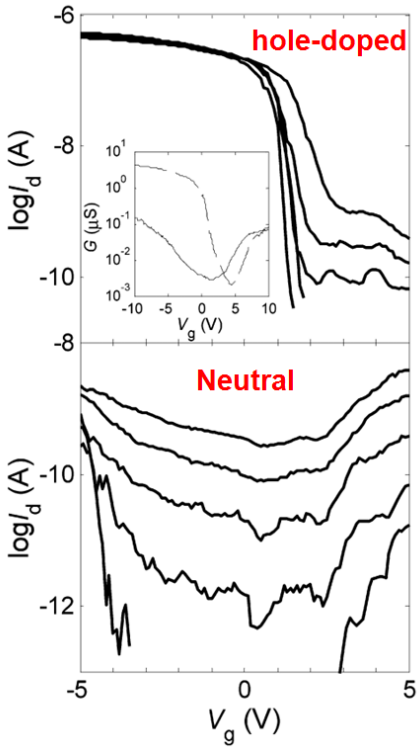

Figure 4.11 Doping dependence of Cr-contacted SWNT FET. Adapted from Ref.[14].

Since the electron doping causes opposite effect to the hole doping described in Fig. 4.11 [12, 14], the model (SB thickening *via* doping) well explains our observation on SB change of Cr-contacted SWNT FET exposed to hydrogen gas (Fig. 4.7b). Figure 4.12 is the schematic diagram of energy band structure explaining the SB thickening *via* doping model [12]. As electron is doped to the SWNT, depletion layer become very thick from dotted line to solid line resulting in the significantly decreased hole injection. Nearly same behavior was shown in step

2 and step 3 of K-doped SWNT of the previous report (Fig. 4.5a) [7]. It indicates that the SB change depending on doping is not a particular case, but more like universal phenomenon.

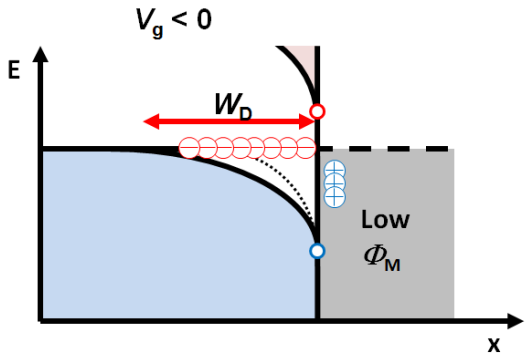

Figure 4.12 Schematic of energy band diagram with negative gate voltage applied. It graphically explains the increase of the depletion layer of SWNT for hole-type charge carrier injection.

4.3.3 H_2 exposure time dependence of I_{ds}-V_{gs} curve shift in different metal contacts

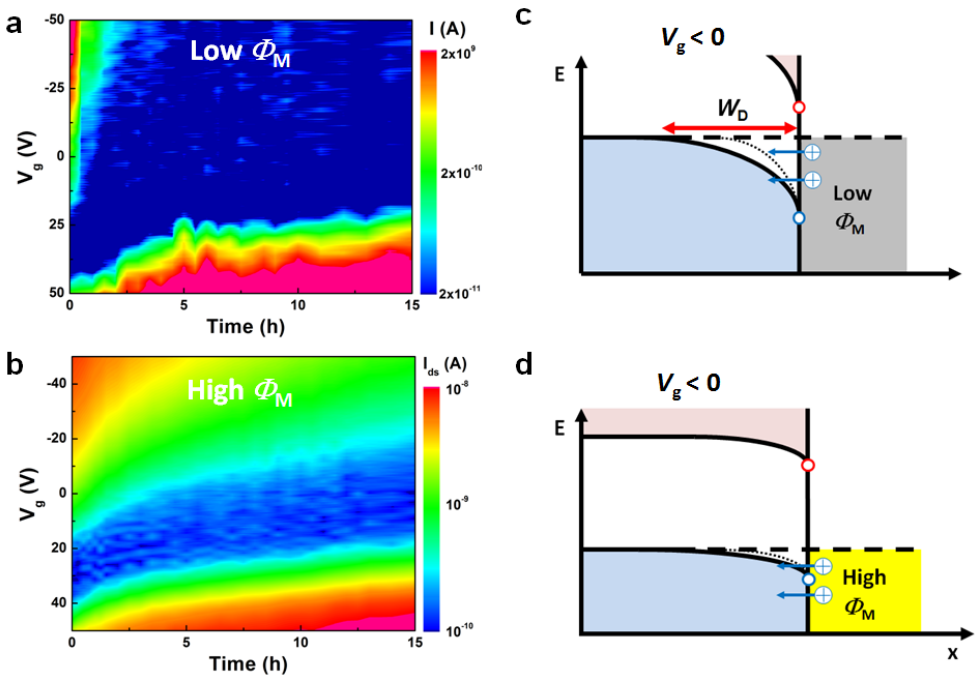

Figure 4.13 H_2 exposure time dependence of I_{ds}-V_{gs} curve shift. Time dependence of (a) Cr (Φ_M = 4.5 eV) contacted SWNT FET and (b) Au (Φ_M = 5.1 eV) contacted SWNT FET. Schematic of energy band diagram of the (c) Cr-contacted SWNT FET, (d) and Au-contacted SWNT FET with negative gate voltage applied for hole injection. The dashed curved line represents the SB of pristine state, and solid curved line represents the thickened SB due to electron doping. Φ_{NT} is work function of the pristine SWNT.

Figure 4.13a is H_2 exposure time dependence of I_{ds}-V_{gs} curve of Cr-contacted SWNT FET. The hole injection to the FET becomes difficult at the very first stage of hydrogen exposure because of increased depletion width as explained before. However, the Au/Ti-contacted SWNT FET did not show that drastic change as shown in Fig. 4.13b. As explained before, most of SWNT is contacted to Au (Φ_M = 5.1 eV) and very short (5 nm) SWNT can contact to Ti (Φ_M = 4.3 eV). When the significant amount of negative voltage is applied, we observed the contact resistance of Ti contact can be very big. In case of $R_{C\text{-}Ti} >> R_{C\text{-}Au} + \Delta R_{SWNT}$, $R_{C\text{-}Ti}$ predominantly decides the total contact resistance [11] because they are forming parallel circuit.

Based on our observation of Figs. 13a and 13b, the huge difference is possibly attributed to the different height of SB from different metal work functions. Figures 4.13c and 13d show the schematic of energy band diagram of the FETs with negative gate voltage applied for hole injection. The dashed curved line represents the SB of pristine state and solid curved line represents the thickened SB due to electron doping. As depicted, the change in depletion layer width may have different effects on the SB with different heights.

There are two main charge transport mechanisms (for hole-type charge carriers depicted in Figs. 4.13c and 13d) in the Schottky type devices, thermionic and tunneling emission [1]. As charge carriers have thermal energy corresponding to k_BT where k_B is the Boltzmann constant and T is temperature, some charge carriers can be excited above the SB and flow by the thermionic emission. While, charge

carriers having energy below the SB also can flow by tunneling (tunneling emission) the SB when drain-source voltage is applied [1].

Because the SB thickening *via* doping significantly affect to the tunneling emission, the low Φ_M metal-contacted device (with 300 meV ~ 500 meV of expected SB height [14]) shows significantly reduced hole current where the tunneling current is the dominant charge transport mechanism (Fig. 4.13c). On the other hand, the high Φ_M metal-contacted device can have one order of magnitude lower SB height [2] that significantly increases the amount of thermionic emission Φ_M [15]. Therefore, the significant amount of the hole injection is possible through the thermionic emission as depicted in Fig. 4.13b [15]. Still, further experiments using same diameter of SWNTs with different contact metals, or statistical approach are needed to check the observed different device responses which really originates from the different metal work functions.

Figure 4.7c is the demonstration of hydrogen exposure process on single strand SWNT contacted to Ti electrodes. Comparing to the Cr-contacted device, Ti-contacted device shows more electron favorable SB formation while hole injection is extremely prohibited as Ti has lower work function (~4.3 eV) than Cr (~4.5 eV). Hence, the thickening (*via* doping) of higher SB in Ti-contacted SWNT effectively prevents the hole injection that cause the leakage current in *n*-type transistor devices. The results are also in accordance with the expected SB formation by the metal work functions [1] and experimental observation [16]. Consequently, we achieved the SWNT FET that nearly perfectly working as an *n*-type semiconductor

by hydrogen exposure to SWNT FET with Ti contacts.

4.4 Summary of Chapter 4

In summary, electron doping effect of Cr- and Ti-contacted SWNT FET exposed to high-pressure hydrogen gas was observed by shifted I_{ds}-V_{gs} curve of *in-situ* 3-terminal electrical measurements. Because the work function of Cr is similar with SWNT, SB thickness change was followed by electron doping effect resulting in significantly reduced hole-type charge carrier transport. Comparing to the Au/Ti-contacted SWNT FET case, we observed noticeable hole carrier reduction after the hydrogen exposure. The huge difference on hole-type carrier injection through Au/Ti-contact and Cr-contact after hydrogen exposure may be attributed to the SB thickness change *via* doping. In other words, the thickness change (*via* electron doping) of higher SB (*via* low work function metal contact) causes significant effect on the I_{ds}-V_{gs} curve. Ti, lower work function metal contact was demonstrated for the realization of reliable *n*-type SWNT FET. Consequently, we achieved the SWNT FET that nearly perfectly working as an *n*-type semiconductor by hydrogen exposure to SWNT FET with Ti contacts.

Bibliography

[1] Svensson J and Campbell E E 2011 Schottky barriers in carbon nanotube-metal contacts *Journal of applied physics* **110** 16

[2] Martel R, Derycke V, Lavoie C, Appenzeller J, Chan K, Tersoff J and Avouris P 2001 Ambipolar electrical transport in semiconducting single-wall carbon nanotubes *Physical review letters* **87** 256805

[3] Meunier V, Souza Filho A, Barros E and Dresselhaus M 2016 Physical properties of low-dimensional s p 2-based carbon nanostructures *Reviews of modern physics* **88** 025005

[4] Guo J, Datta S and Lundstrom M 2004 A numerical study of scaling issues for Schottky-barrier carbon nanotube transistors *IEEE Transactions on Electron Devices* **51** 172-7

[5] Chai Y, Hazeghi A, Takei K, Chen H-Y, Chan P C, Javey A and Wong H-S P 2011 Low-resistance electrical contact to carbon nanotubes with graphitic interfacial layer *IEEE Transactions on Electron Devices* **59** 12-9

[6] Zhang Z, Wang S, Wang Z, Ding L, Pei T, Hu Z, Liang X, Chen Q, Li Y and Peng L-M 2009 Almost perfectly symmetric SWCNT-based CMOS devices and scaling *ACS nano* **3** 3781-7

[7] Radosavljević M, Appenzeller J, Avouris P and Knoch J 2004 High performance of potassium n-doped carbon nanotube field-effect transistors *Applied Physics Letters* **84** 3693-5

[8] Do Thanh L and Balk P 1988 Elimination and Generation of Si-SiO2 Interface Traps by Low Temperature Hydrogen Annealing *Journal of The Electrochemical Society* **135** 1797-801

[9] Kybert N J, Lerner M B, Yodh J S, Preti G and Johnson A C 2013 Differentiation of complex vapor mixtures using versatile DNA–carbon nanotube chemical sensor arrays *ACS nano* **7** 2800-7

[10] Makaram P, Selvarasah S, Xiong X, Chen C-L, Busnaina A, Khanduja N and Dokmeci M R 2007 Three-dimensional assembly of single-walled carbon nanotube interconnects using dielectrophoresis *Nanotechnology* **18** 395204

[11] Lan C, Srisungsitthisunti P, Amama P B, Fisher T S, Xu X and Reifenberger R G 2008 Measurement of metal/carbon nanotube contact resistance by adjusting contact length using laser ablation *Nanotechnology* **19** 125703

[12] Léonard F and Tersoff J 1999 Novel length scales in nanotube devices *Physical review letters* **83** 5174

[13] Lide D R 2004 *CRC handbook of chemistry and physics* vol 85: CRC press)

[14] Chen Y-F and Fuhrer M S 2006 Tuning from thermionic emission to ohmic tunnel contacts via doping in Schottky-barrier nanotube transistors *Nano letters* **6** 2158-62

[15] Svensson J, Sourab A A, Tarakanov Y, Lee D S, Park S J, Baek S J, Park Y W and Campbell E E 2009 The dependence of the Schottky barrier height on carbon nanotube diameter for Pd–carbon nanotube contacts *Nanotechnology* **20** 175204
[16] Tseng Y-C and Bokor J 2010 Characterization of the junction capacitance of metal–semiconductor carbon nanotube Schottky contacts *Applied Physics Letters* **96** 013103

Chapter 5

Conclusion

We report changes in the electrical property of SWNT caused by exposure to high-pressure hydrogen. First, we report the electron doping effect of SWNT. *In-situ* 3-terminal electrical measurements with hBN substrate were used to observe the intrinsic electronic properties of hydrogen-exposed SWNT. Comparing to the planar graphene sheet device, we observed the curved structure of SWNT is advantages on the reaction with hydrogen molecules. XPS and Raman spectroscopy verified the formation of C-H bond on SWNT surface after the hydrogen exposure process. The covalent bond yielded short-range scattering in the graphene device and band gap widening in the SWNT devices.

Second, the metal work function-dependent doping effect on SWNT FET is investigated. To obtain the SWNT FET with higher Schottky barrier (SB) for the hole injection, we adapted the different contact metals that have lower work functions such as Cr and Ti replacing the Au/Ti electrodes. Comparing to the Au/Ti-contacted SWNT FET case, we observed noticeable hole carrier reduction after the hydrogen exposure in Cr- and Ti-contacted devices. It suggest the doping induced SB thickness change relies on the SB height. In other words, the changes

in thickness (*via* electron doping) of higher SB (*via* low work function metal contact) causes more significant effect on the I_{ds}-V_{gs} curve. Consequently, we achieved the SWNT FET that nearly perfectly working as an *n*-type semiconductor by hydrogen exposure to SWNT FET with Ti contacts.

Since the electron doping effect was also reproduced in SWNT network devices, we expect the useful electrical properties and the stable nature of C-H bond observed in the hydrogen-exposed SWNT can leads a step forward to the application of SWNT for the next generation electronics.

국문초록

탄소나노튜브 (CNT)는 차세대 전자 소자로 가장 유망한 물질 중 하나로 손 꼽힌다. 하지만 CNT 기반 전자공학을 실현하기 위한 몇 가지 장애물들이 존재한다. 특히, 공기 중에서 *p*형 반도체 성향을 강하게 띠는 것이 문제이다. 집적회로를 구성하기 위해서는 *n*형 도 필요하다. 따라서 안정적으로 작동하는 *n*형 CNT 트랜지스터의 개발이 요구되고 있다.

이 논문에서는 단겹 탄소나노튜브 (SWNT) 를 고온 고압 수소에 노출 시킨 뒤 변화하는 전기적 특성을 소개 한다. 첫 번째로는 전자 도핑 현상을 보고한다. 2차원 부도체이자 불포화 결합이 최소화 된 것으로 알려진 hexagonal boron nitride 기판을 사용한 소자를 제작하여 기판으로부터 야기되는 외부 환경의 영향을 최소화 하였다. 뿐만 아니라 이 소자의 수소 노출 전 과정을 *in-situ* 측정법으로 측정하여, 외부 환경에 의한 영향을 배제한 SWNT 고유의 전기적 특성을 측정 할 수 있었다. 그 결과, 수소에 노출된 SWNT에 전자가 도핑 되는 현상을 관측하였다. SWNT의 곡률이 수소와의 반응에 이점으로 작용한다는 결과를 평면 구조인 graphene 소자와의 수소노출 비교실험에서 확인 할 수 있었다. 엑스선 광전자 분광법 와 라만 분광법을 통해 고온, 고압에 노출된 SWNT에 C-H 결합이 화학적으로 생성된 것을 확인 하였다. 마지막으로 이 공유결합에 의해 graphene에서는 short-range scattering 현상이, SWNT 에서는 에너지 밴드 갭 확장 현상이 관측 되는 것을 확인하였다.

두 번째로 SWNT 전계 효과 트랜지스터 (field effect transistor, FET)의 전기적 컨택을 변화하는 연구를 진행하였다. SWNT와 금속 컨택에서 발생하는 쇼트키 장벽의 높이가 금속과 SWNT의 일 함수 차이에 의존하기 때문에, 금 보다 낮은 일 함수를 갖는 금속인 크롬, 티타늄을 전기적인 컨택 물질로 사용하여 그 차이점을 연구한 것이다. 그 결과 일 함수가 낮은 크롬, 티타늄을 컨택으로 사용 했을 때 금을 사용한 경우보다 훨씬 적은 양의 홀(hole) 타입 전류가 흐른다는 사실이 관측되었다. 이 관측을 통해 전자 도핑으로 인해 야기된 쇼트키 장벽의 두께 변화의 영향이 쇼트키 장벽의 높이에 의해 크게 좌우 될 수 있다는 것을 알 수 있다. 즉, 크롬과 티타늄과 같이 높은 쇼트키 장벽을 갖는 금속 컨택의 경우에, 전자 도핑에 따른 쇼트키 장벽의 두께 증가가 크게 나타나 홀 타입 전류를 크게 감소시킨다는 것이다. 따라서 우리는 이 현상을 이용하여 거의 완벽하게 *n*형 트랜지스터로 작동 하는 SWNT FET를 제작 할 수 있었다.

수소에 노출된 SWNT에 형성된 안정적인 C−H 결합에 의한 전자 도핑 현상이 SWNT 네트워크 소자에서도 나타남을 확인 함으로써, 앞으로 이 기술이 대 면적 나노튜브 소자의 전자 도핑에 응용될 수 있음을 확인하였다.

주요어 : 탄소 나노튜브, 수소화, 전자 도핑, *n*형 트랜지스터, 전기적 측정, 전기 접촉, 쇼트키 장벽

학번 : 2012−23086